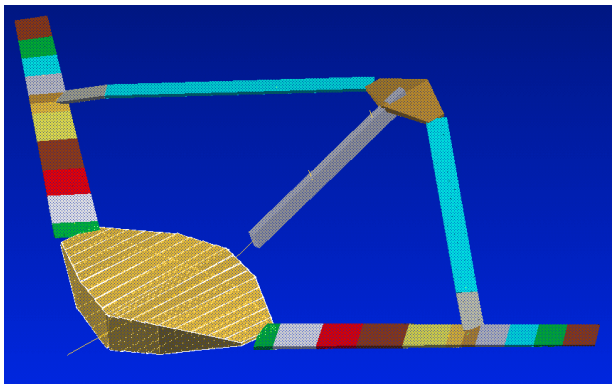

Evaluation of structural parameters on linear/non-linear design spaces of the Joined Wing Sensorcraft

André Luís Gomes Coelho

Thesis to obtain the Master of Science Degree in

Aerospace Engineering

Supervisor: Prof. Afzal Suleman

Examination Committee

Chairperson: Prof. Fernando José Parracho Lau

Supervisor: Prof. Afzal Suleman

Member of the Committee: Dr. Frederico José Prata Rente Reis Afonso

March 2016

Acknowledgments

First of all, I would like to thank my primary supervisor, prof. Afzal Suleman, for give me the opportunity to be a part of an interesting project as the Joined Wing Sensorcraft.

I would also like to thank the persons who give me some help or advices during the development of this work when I was in Quaternion Aerospace. They are Jenner Richards, Ryan Flagg, Willem Brussow and Casey Keulen.

Last and the most important, I would like to thank to my family including my girlfriend, for all they have done in all fields of my life to turn this thesis possible.

Without all of these supports I would never had complete my thesis, thank you to all.

Resumo

A Força Aérea dos Estados Unidos solicitou uma aeronave capaz de transportar conjuntos de sensores avançados sobre distâncias muito grandes e em altitudes extremas. Para atingir esses objetivos, é necessária uma aeronaves não convencional. O *Joined Wing Sensorcraft*, da Boeing™, pode ser a solução para este problema. Embora, possam existir riscos com esta abordagem, como por exemplo a instabilidade devido a não-linearidade geométrica, que normalmente não são investigados em projetos preliminares.

Nesta tese, diferentes parâmetros estruturais foram explorados, a fim de entender o comportamento deste tipo de configuração. Os parâmetros que serão focados são as articulações e a rigidez dos membros que compõem a aeronave.

Análises de sensibilidades e *carpet plots* foram gerados em estudos lineares e não-lineares. Durante o desenvolvimento deste trabalho serão mostrados três tipos diferentes de não-linearidades geométrica que podem ocorrer com este tipo de estrutura.

Para realizar este estudo, a correspondência de um modelo de alta fidelidade com um modelo de vigas simplificado é necessária, a fim de diminuir o tempo para gerar o espaço de *design*. Além disso, alguns teste estáticos no avião e também testes dos materiais foram feitos para identificar o quão bem o modelo de alta fidelidade é comparado com o UAV real, já produzido.

Palavras-chave: Joined Wing; Sensorcraft; UAV; parâmetros estuturais; análises de sensibilidade

Abstract

The United States Air Force requested an aircraft capable of transporting sets of advanced sensor over very large distances and at extreme altitudes. To achieve these objectives, an unconventional aircraft is required. The Joined Wing Sensorcraft, from Boeing™, maybe the solution to this problem. Although, this new design could have instabilities due to geometric nonlinearity not normally investigated in preliminary design phases.

In this thesis, different structural parameters were explored in order to understand the behaviour of this type of configuration. The parameters that will be focus on are the joints and the stiffness of the members that compose the aircraft.

Sensitivity analyses and carpet plots were generated on linear and non-linear analysis. During the development of this study, it was found three different types of geometric nonlinearity that can occur with this type of structure.

To carry out this study, matching a high fidelity model with a simplified beam model is needed, in order to decrease the time to generate the design space. Furthermore, a few static tests on the airplane and also material tests were made to identify how accurate the high fidelity model is when compared with the actual UAV already produced.

Keywords: Joined Wing; Sensorcraft; UAV; structural parameters; sensitivity analysis

Table of Contents

List of tables

List of figures

List of acronyms and symbols

AFRL	Air Force Research Laboratory
CAD	Computer-Aided Design
DOC	Direct Operating Cost
DOE	Design of Experiments
E	Young Modulus
FEA	Finite Element Analysis
FEM	Finite Element Model
FW-RW	Forward and Rearward
g	Gravity Acceleration
GSRPV	Geometrically Scaled Remotely Piloted Vehicle
HALE	High Altitude and Long Endurance
HF FEM	High Fidelity Finite Element Model
I	Moment of Inertia
ISR	Intelligence Surveillance and Reconnaissance
J	Polar Moment of Inertia
JWSC	Joined Wing Sensorcraft
K^e	Stiffness Matrix
L	Length of element
LC	Load Case
LS	Load Step
MOI	Moment of Inertia
NASA	National Aeronautics and Space Administration
NL	Non-Linear
RPV	Remotely Piloted Vehicle
RSM	Response Surface Methodology
UAV	Unmanned Aircraft Vehicle
US	United States
Φ	Shape Functions

1. Introduction

1.1. SensorCraft – Background

SensorCraft is the name given to for a high altitude and long endurance (HALE) unmanned aerial vehicle (UAV), capable of providing revolutionary intelligence, surveillance, and reconnaissance (ISR) in military and civil sectors when equipped with advanced sensor packages [1].

Nowadays, constant surveillance over vast geographic areas is a vital point in military missions. Due to this fact, the Air Force Research Laboratory (AFRL) is developing the SensorCraft concept to have a solution for constant battle space awareness [2]. In order to do so, the SensorCraft should be able to stay in missions for more than 30 hours plus has the capability of covering a maximum range of 2000 nautical miles [3]. Figure 1.1 shows the SensorCraft mission profile.

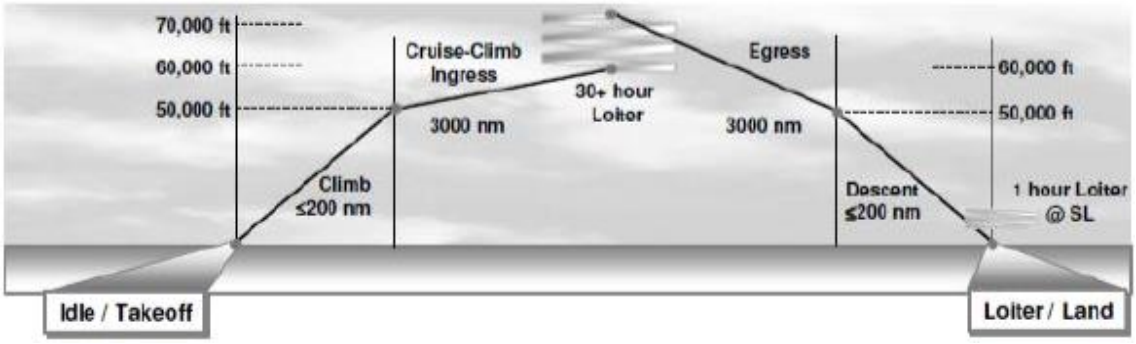

Figure 1.1 - SensorCraft Mission Profile [3]

To respond to these objectives, different companies presented different concepts (Figure 1.2). Lockheed Martin™ presents a wing-body-tail that it is a conventional large aspect ratio design. Northrop Grumman proposed a flying wing design. And Boeing™ brought back to study a Joined-Wing configuration, which is made of a wing pair: forward and aft wings connect to each other forming a diamond shape [4].

Figure 1.2 - Lockheed Martin Concept (left); Northrop Grumman concept (middle); Boeing Concept (right) [3]

In order to understand better the behaviour of this unconventional design (Joined Wing), NASA, US Air Force, US Navy and Boeing™ have been studied this concept for several years in different designs.

To accomplish the primary objective of surveillance, the Joined Wing SensorCraft (JWSC) provides the ability of 360 degrees surveillance, by embedding sensor packages in both wings, forward and aft wings, which is a huge advantage over others designs (Figure 1.3) [2].

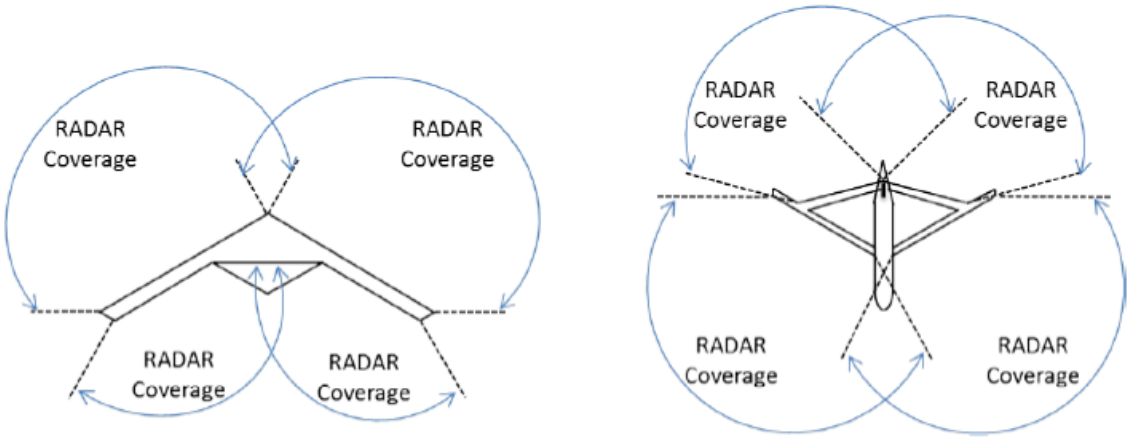

Figure 1.3 – Sensor packages on conventional wing and Joined Wing [2]

According to Wolkovith, it is possible to reduce about 30% of the wing structural weight and 5% on the induced drag when compared with a conventional wing-body-tail configuration [6].

JWSC have the capability of implementing aerodynamic control surfaces on both wings (Figure 1.4) [7]. This creates a control system completely new, which has the possibility of sliding or curving without rolling while maintaining the antennas in the same azimuth plane (Figure 1.5).

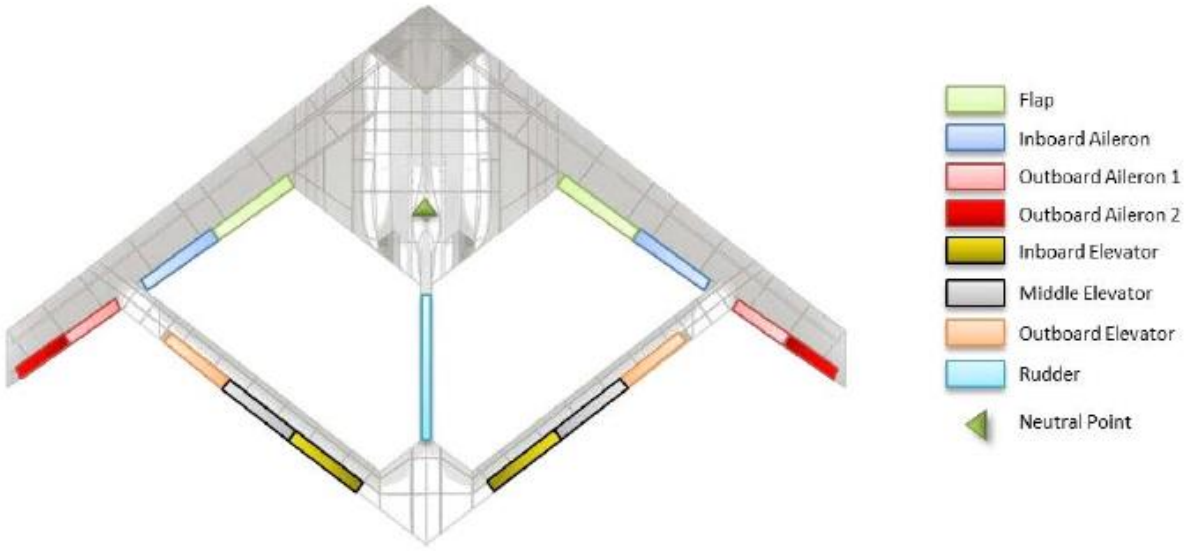

Figure 1.4 - Control surfaces of JWSC [7]

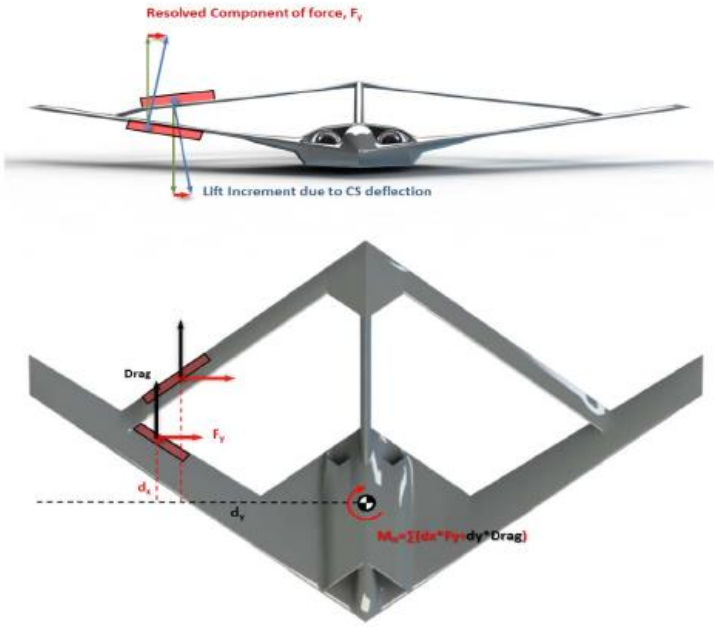

Figure 1.5 - Effect of resolved lift increment on aircraft yaw [7]

Another point in favour of this concept is to take advantage of the Wolkovitch's effect [6], which will be explained in next paragraph.

The bending axis of this configuration is tilted because the structure of the aircraft is a truss. Due to the tilted bending axis of the aircraft, which is normal to the plane defined by the forward and aft wing, the material must be concentrated in the upper leading edge of the spar and the lower trailing edge of the spar (Figure 1.6A). The optimum design for the wing box of the JWSC has the leading edge spar as far forward as possible and the aft spar as aft as possible which create more empty space for fuel and choice of a thinner airfoil, reducing weight and giving the possibility for a better transonic performance (Figure 1.6B) [4].

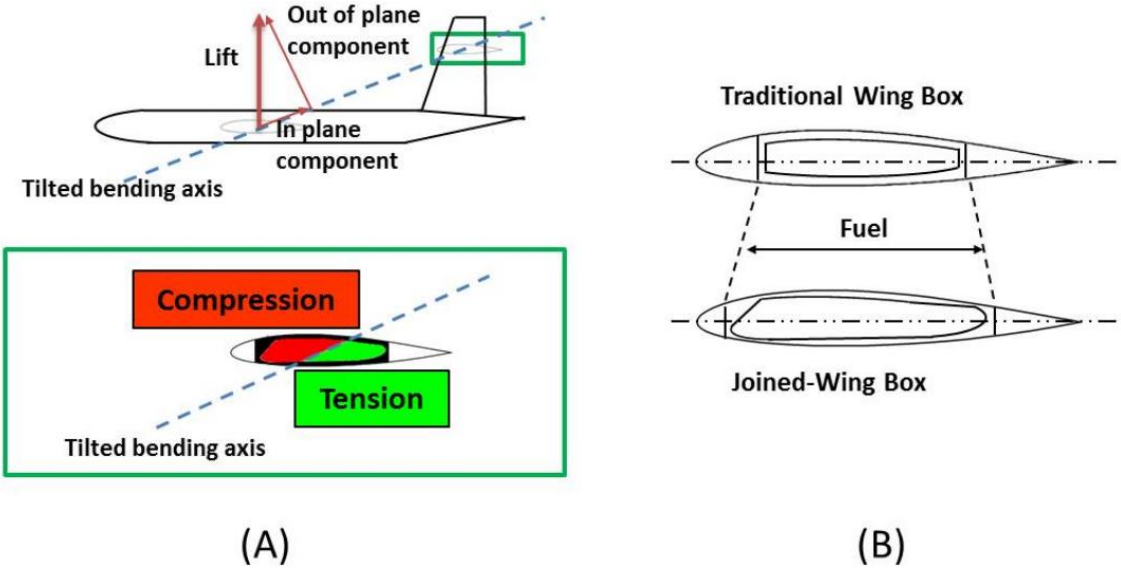

Figure 1.6 - (A) Tilted bending axis of joined wing configuration; (B) Wing Box Comparison [4]

It has discovered from computational studies that JWSC has the possibility of presenting a nonlinear structural response, due to large deflections on the wings, which can cause a collapse of the structure. Indeed, buckling could appear in forward and aft wings. In the next sub-chapter, the most important studies and conclusions in the author opinion are presented.

1.2. Previous Study

In 1986, Julian Wolkovitch was the first person to present the joined wing concept as it is known today when he published [6]. He demonstrated the importance of optimization between structure and aerodynamics to archive all the advantages that this configuration can brings.

After 14 years, in 1990, Kroo, Gallman, and Smith extended Wolkovitch's design exploration by completing a more detailed aerodynamic and structural studies. They show that using an asymmetric material distribution in spar is the key point to have the Wolkovitch's effect. In their studies, they researched the buckling in the aft wing, which suggested the need for a nonlinear analysis [8]. The same authors preformed an optimization of the aircraft design comparing this with a conventional aircraft configuration for a medium-range transport mission profile. Firstly, the direct operating cost (DOC) was 2% smaller for the Joined-Wing configuration. Although, when they added the buckling constraint for the Joined-Wing configuration, the DOC of the conventional transport aircraft became smaller (3.2%) than the Joined-Wing [9]. In 1996, Gallman and Kroo researched an optimized joined-wing configuration by performing a nonlinear structural analysis. With this last study, they concluded that the joined-wing configuration is heavier than a traditional configuration and the factor responsible for this result was the inclusion of the buckling constraint in the optimization [10].

For many years, the development of the knowledge about joined-wing configuration was set aside. However, after the changing of the millennium, the increasing demand for UAVs, the more advanced computational tools and the better materials has brought back the study of this configuration as prove the Boeing^{TM}'s choice.

Several studies were performed at beginning of this century [11] [12] [13]. All of these studies are about the nonlinear structural and aeroelastic behaviours of the joined-wing aircraft. After all, transient analyses were recommended for archiving all the physic around joined-wing configuration [13].

In 2005, Roberts, Canfield, and Blair set the objective of creating a structural model that is nonlinearly optimized and aerodynamically trimmed. They developed their software and model configuration in order to match the desired objective [14]. In their models, they included a buckling analysis on the resulting optimized model. The authors discovered that the critical load condition throughout the design process was the manoeuvre speed gust load. After that, their results showed large geometric nonlinearity near the critical buckling eigenvalue in the form of aft wing buckling. Due to this fact, the conclusion was that the nonlinear analysis is critical to correctly capture the aero-structural responses of the joined-wing configuration. The same authors also published an article related to the ability of archiving a structurally optimized and aerodynamically trimmed conceptual

joined-wing design, while including geometric nonlinearities [15]. The result from these studies proves that the forward wing is able to buckle like the aft wing.

Vanessa Bond was the first to experimentally test the joined-wing configurations in 2008. The goal of Bond's research presented in her dissertation was to experimentally validate the feasibility of including aft wing twist in the joined-wing configuration for pitch control [16]. An important aspect of this research was the consideration of nonlinear response for the configuration. She concluded that controlling the aft wing twist can also control the pitch of the aircraft, then are uncontrolled aft wing twist could have serious implications on the longitudinal stability of the aircraft, due to this fact, the nonlinear analyses are extremely important to study the joined wing. In her static test, she demonstrated that the following forces have significant influence on the response of joined-wing.

After proving the nonlinearity of this configurations in static tests, the AFRL requested a 1/9th scale remotely piloted vehicle (RPV) of the Boeing joined-wing SensorCraft to be constructed and flown [4]. In Figure 1.7, it is possible to see the dimensions of the proposed Boeing™ SensorCraft and a comparison with a bomber aircraft, the B-2. Also, in Figure 1.8 it can be seen the 1/9th scale RPV compared with the baseline and also with a person.

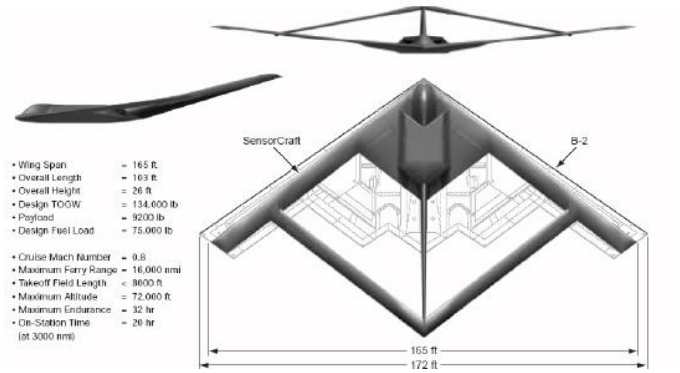

Figure 1.7 - Boeing™ SensorCraft view and comparison size with B-2 [3]

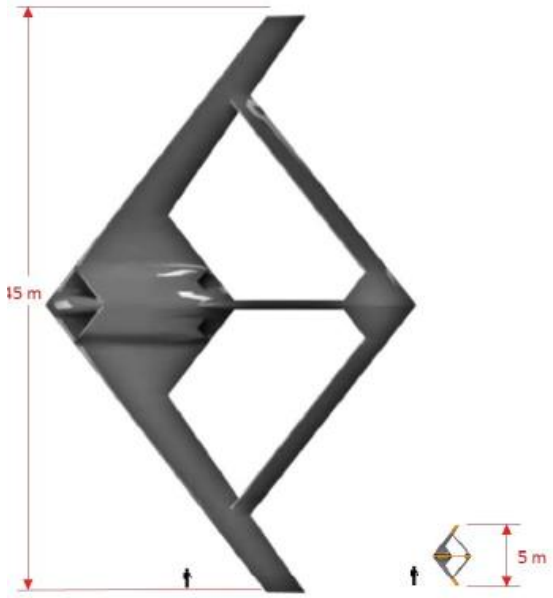

Figure 1.8 - Relative Scale of Boeing™ Baseline Aircraft and the 1/9th scale RPV [7]

The AFRL has the objective of observing geometric nonlinearities and aeroelastic responses in flight [4]. This task was first investigates by Richards [13]. The first fight (Figure 1.9) of the Geometrically Scaled RPV (GSRPV) took place in Foremost, Alberta on Saturday October 15th, 2011 with the duration of 7 minute and 58 second in the air [17]. This experiment was the proof that the joined-wing, one marginally unstable aircraft, has the ability to successfully operate [4].

Figure 1.9 - GSRPV in flight (left); After flight (right) [4]

In 2013, Jeffrey in his master thesis demonstrated with experimental tests that the GSRPV would not support the required ultimate load due the buckling failure of the forward wing. He and Richards proposed for the future an optimized aft wing and a stiff vertical boom which generate the flexibility of the forward wing [4].

1.3. Thesis Summary

After the presentation of the Joined-Wing concept, the chronological developments and investigations related to this configuration, and the project of the JWSC that AFRL requested, appear the body of this thesis.

First of all, the results from the experimental static tests in the GSRPV made in Quaternion Aerospace are presented. These results will be used to match the High Fidelity Finite Element Model (HF FEM) of Jenner Richards [13], using joint connections and material properties as variables. Also, sensitivity studies of these variables were performed.

Regarding the tests of the material properties, the productions of the composite coupons were explained and next the setup of the experimental tests was described.

With the results of HF FEM, a simplified beam model was created in order to perform sensitivity studies assess the influence of the different body part stiffness, such as forward and aft wings, fuselage and boom.

After that, an introduction to recent software named ModelCenter™ of Phoenix™ and also the ability to create the optimization process were described.

This thesis goal was not to the research which is the best optimization algorithm for a situation either the mathematical background of it, although some important ideas were taken into account.

Finally, the results of this study are presented and commented. Also, the conclusions were drawn and future a development is suggested.

2. Static test of the Joined Wing Sensorcraft

In the beginning of the project, several static tests were performed to investigate the response of prototyped aircraft. These static tests are described in the next chapter.

The first test will be to discover which are the deflections of the forwards wings and the boom. To do that, the aft wings will be detached from the aircraft (Figure 2.1). A symmetry load will be applied on the forward wings and the tip displacement of each side, right and left, were written down in a vertical tube. To prevent the airplane from lifting, sand bags were stack above the fuselage.

Figure 2.1 - Static Test Forward Wings Load

The load will be applied using a wood beam that will transfer the load from a suspended bucket to the wings. The bucket has some sand bags and/or lead spheres that will create the force which will be transfer to the forward wing, half of the total load on the bucket is applied to each wing. To determine the displacement on the wing tips, two pillars were put in each side of the wings. Increment loads were applied.

To investigate the boom deflection, the same strategy was followed, although on this static test a direct load was applied to the structure (Figure 2.2).

Figure 2.2 - Static Test Boom Load

After testing the forward wing and boom, it is time to include the aft wing to create the diamond shape. The experience will be performed in the same way as before. And the measurements of the forward wings tip and the boom will be taken for each load step (Figure 2.3).

Figure 2.3 - Static Test with Aft Wings, Boom Load (left), Wing Load (right)

2.1. Experimental Results

The results for these two static tests are plotted in Figure 2.4. These tests show a linear behaviour of the aircraft structure. Although, the right and left wing have different displacements, for the optimization an average value was considered. The first thought of the factor that creates these non-symmetrical values was the rotation of the fuselage, but as Jeff [4] proved using a much more precise static test that these discrepancies between the stiffness of right and left forward wing persisted. The causes of this asymmetric behaviour could be due to the manufacturing issues, different orientation of the fibres, different load applied and many other factors.

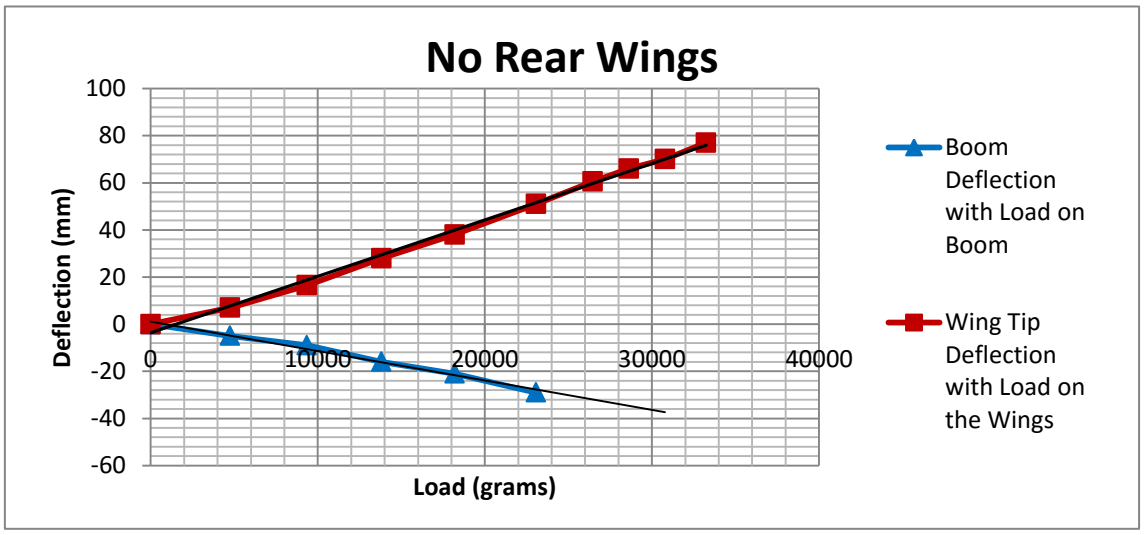

Figure 2.4- Results for the Static Test without the Aft Wings

The results for the boom load and wing load, when the aircraft is fully assembled, are presented in the next figures.

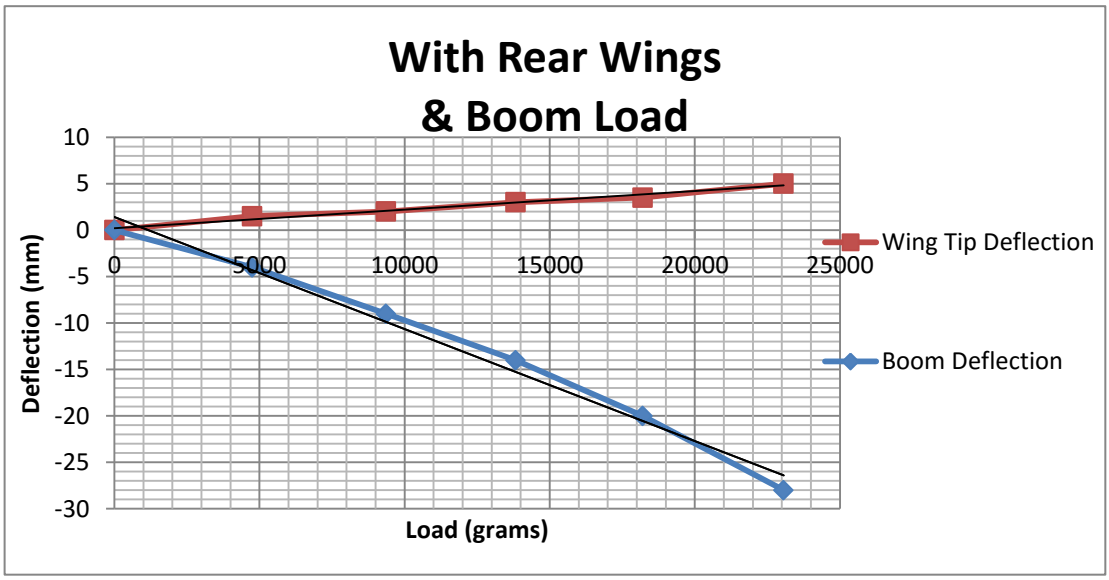

Figure 2.5 - Results for the Boom Load with Aft Wings

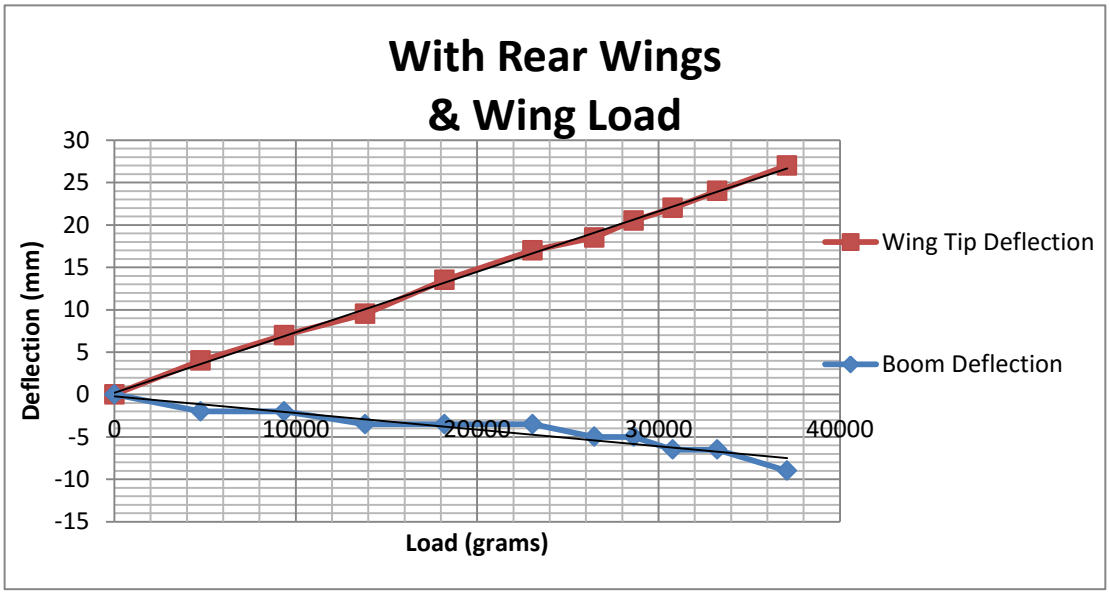

Figure 2.6 - Results for the Wing Load with Aft Wings

Regarding these results, for the boom load it can be seen a non-linear behaviour on the boom displacement. The stiffness of boom increased a small amount (5%) with the aft wing attached.

With the wing load, the boom displacement was so small that make it difficult to obtain the exact value. The stiffness of wing was increased significantly (66%) with the aft wing attached.

2.2. Comparison of High Fidelity Model and Experimental Results

To check the accuracy of the high fidelity model made by Jenner Richard [18] a comparison with experimental results were done.

To have the realistic displacement two load steps were simulated. In the load step1 (LS1) just the gravity was taken into account, in load step2 (LS2) the gravity and the load were implemented. The difference for the displacement in zz direction between these load steps was the value to consider in the comparison with the realistic test. Next equation (1) shows how the displacements for high fidelity model were calculated.

$$displacement = displacement\ (LS2) - \ displacement\ (LS1) \qquad (1)$$

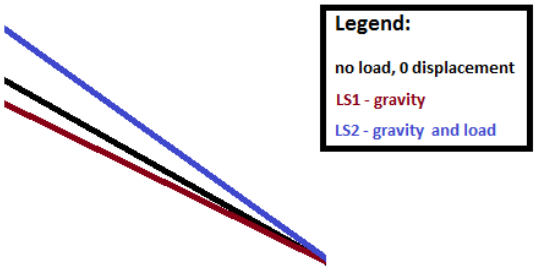

Figure 2.7 - Scheme of the forward wing displacement for both load steps

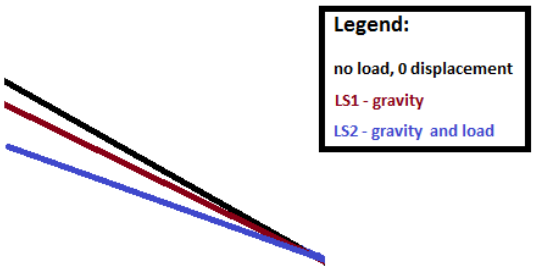

Figure 2.8 - Scheme of the boom displacement for both load steps

Figure 2.9 shows the displacement of the HF FEM for the two load steps when the load is applied to the wings. These are the type of plots that were generated by ANSYS™.

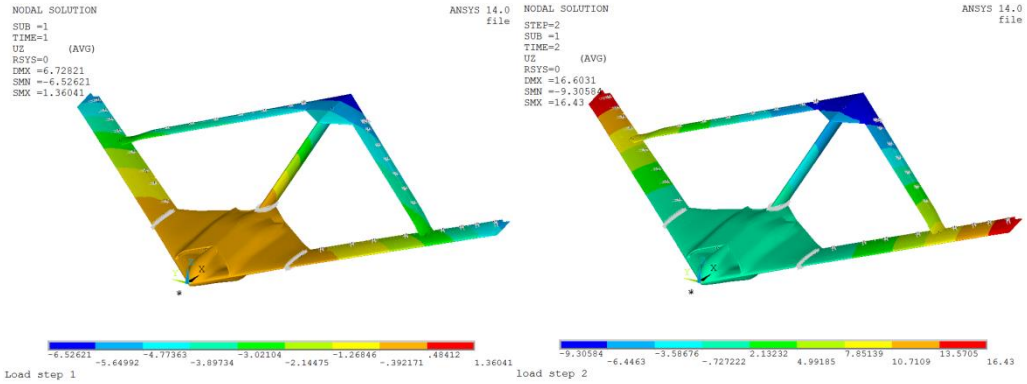

Figure 2.9 - High Fidelity Model: displacement plots [mm] for both load steps with load on wings, LS1 (LHS), LS2 (RHS)

Next a comparison of the experimental results and the HF FEM is presented, without the aft wings (Table 2.1) and with the aft wings (Table 2.2).

No Rear Wings				
Load on	**Load *[Kg]***	**FEA def. *[mm]***	**exp. def. *[mm]***	**relative error to exp.**
wing	33.24	53.08	77	-31.1%
boom	23.06	5.42	29	-81.3%

Table 2.1 - Comparison of the High Fidelity Model and Experimental Results for Loads without Aft Wings

With Rear Wings							
Load on	**Load *[Kg]***	**FEA def. *[mm]***		**exp. def. *[mm]***		**relative error to exp.**	
		boom	**wing**	**boom**	**wing**	**boom**	**wing**
wing	33.24	0.62	15.12	6.5	24	-90.5%	-37.5%
boom	23.06	5.44	6.58	28	5	-80.6%	31.6%

Table 2.2 - Comparison of the High Fidelity Model and Experimental Results for loads with Aft Wings

These experiences reveal that the FEA model is stiffer than the real model, which is a dramatic result due a possible failure that the FEA model cannot predict, and so this FEM is not aa conservative as it should be. There are many factors that can lead to this result such as the material properties, the manufacture constraints and even the joints, without mentioning about mistakes that can happen in experience and in finite element modulation.

Next point to study will be the modulation of joints. Until now, the joints were considered as rigid elements, although an investigation is required to see how these elements influence the overall

stiffness of the full model. The modulation of joints as universal joint element is required, and it is here that ModelCenter™ can be a powerful tool. In parallel, some test coupons were made to investigate if the material properties of carbon and glass fibre are correct.

2.3. Match Joint Stiffness for the Experimental Results

In order to match the experimental results with the joints as design variables, a project was created in ModelCenter™ as illustrated in Figure 2.10. First of all, a database for the load case was generated in an excel spread sheet, and then a module which has all the variables, in this cases just the joint values. The load inputs and values for joints are connected to an Ansys™ module that will run the finite element code and then output the displacements. This last will be the input for a spread sheet that calculates the error of the run model. Finally, ModelCenter™ storage all the values of each run and this program using an optimization code choose by the user will compute the next inputs. The optimization used was Darwin Algorithm. The focus of this thesis was not the background of optimization algorithms, although the choice of this algorithm was because with this kind of algorithm it is possible to have the best value in the optimization space without staying in a local minimum although this choice has a huge cost in iterations and time.

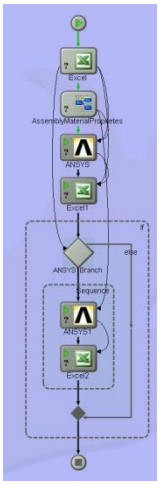

Figure 2.10 - High Fidelity project in Modelcenter™

An idea was needed to implement the best way to match all the design variables and have the best results possible. To start, we need to try to separate design variables from each other, and solve one at the time, this will improve the speed of optimization. Using the Sensorcraft configuration without the rear wings and the load/results for the experimental test, it is possible to isolate the fuse/forward wing joint and the fuse/boom joint.

After that and using the aircraft with rear wings attached, the system will have two variables: forward/rear wings and boom/strake joints, and two load case, wings and boom load. This optimization was performed using two design variables and two objectives which are the deflection of wings and

boom with respective loads because now the wing and boom displacement depend on each other. The objective is to minimize the error in wings tips and boom at the same time.

The Figure 2.11 summarizes these ideas.

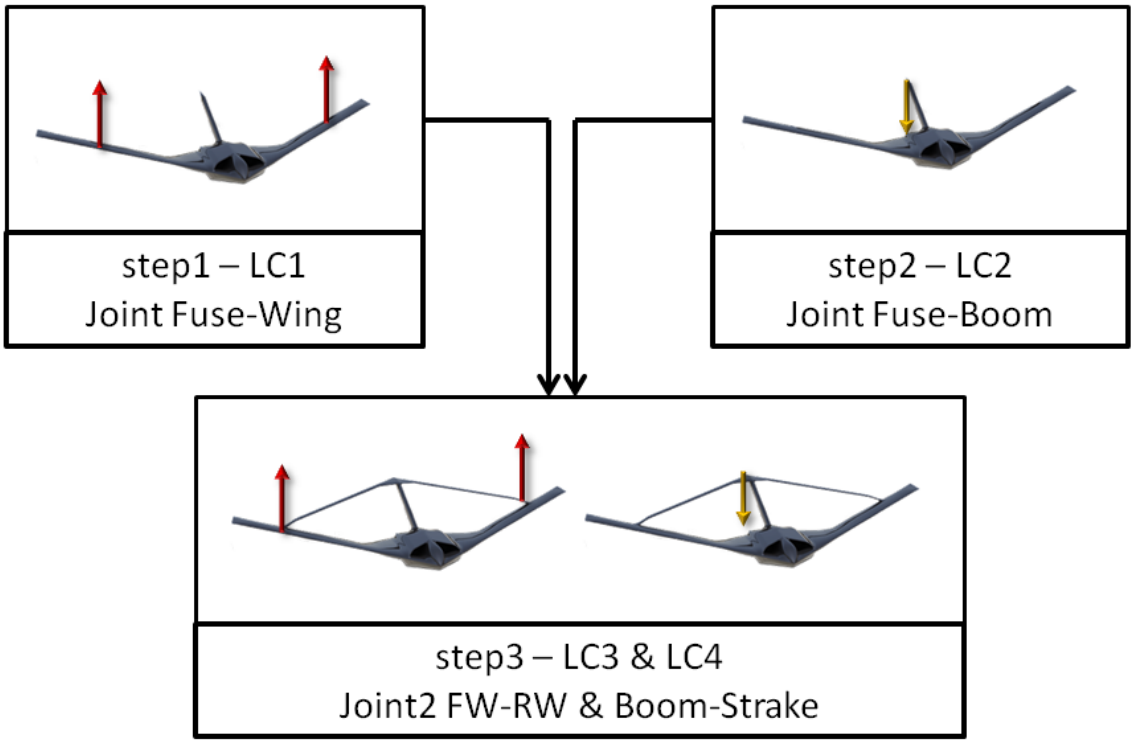

Figure 2.11 - Steps for the Optimization of the Joints on Sensorcraft

After the optimization processes were completed, the joints came up with values represented in Table 2.3. In this table, the error relative to experimental results is presented.

Joint	Joint *[Nmm/rad]*	Loadcase	relative error to experimental	
			boom	wing
Fuse-Wing	166000	1	N/A	0.4%
Fuse-Boom	6400	2	0.0%	N/A
FW-RW	1000	3	84.8%	12.2%
Boom-Strake	10000	4	61.5%	81.3%

Table 2.3 - Values for Joints and relative error to experimental results using an optimization of the High Fidelity Model

The result for step1 of the optimization was an error value of 0.4% with this deviation of the results of both wing tips due to the asymmetry of the model. Step2 shows that it is possible to get an error of 0% and get the perfect solution. This is a straight forward optimization, one response and one objective. In other hand, for step3 the optimization shows a huge error, and needs a detailed view.

In Figure 2.12 are represented two graphics where it is possible to see the evolution of responses and inputs with the iteration process. The boundaries for the design variables, FW-RW and Boom-Strake joints, are 500 and 10000 [Nmm/rad] respectively for the lower and upper boundaries.

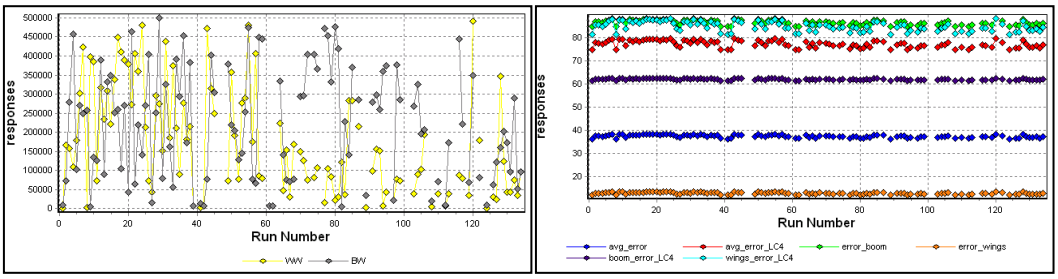

Figure 2.12 - Step3 Inputs (left); Outputs (right)

In conclusion, it is possible to see that the outputs have a small influence with the inputs of FW-RW and Boom-Strake joints. In order to improve the results, another optimization process was performed. This time, all joints will be used in a single optimization for load case 3 and 4. And after that, it is needed to be checked the results for load case 1 and 2. Table 2.4 shows the relative error to the experimental results for this optimization using only the step 3 on the first process.

Joint	**Joint *[Nmm/rad]***	**Load case**	**relative error to experimental**	
			boom	**wing**
Fuse-Wing	170000	1	N/A	13.8%
Fuse-Boom	200000	2	71.0%	N/A
FW-RW	185000	3	17.1%	39.7%
Boom-Strake	185000	4	39.5%	15.8%

Table 2.4 - Values for the Joints and the relative error to experimental using an optimization of High Fidelity Model with all joints at same time

Comparing the different optimization process, it can been seen that with the first one, it is possible to have a zero error for step1 and step2, which is a perfect match, although when the structure has the aft wing on, the coupling of the results reveals to be worse than using the second optimization.

Only for the step2, where the load is applied to the boom and the aircraft has not the rear wings assembled, the error is almost the double of the worse second value. It is not possible only with the joints to match the experimental results.

2.4. Test Coupons & Sensitive Study of Material Properties

After the optimization of the joints for the high fidelity model, which revealed some results that were not expecting, it was decided that there are another variables that could cause the difference. These variables are the material properties that were implemented in the high fidelity model. In order to verify if the values are acceptable, some test coupons were produced. These coupons were created by follow the documentation “Tensile test specimen preparation” [19].

Figure 2.13 shows two pictures of the production of these test coupons.

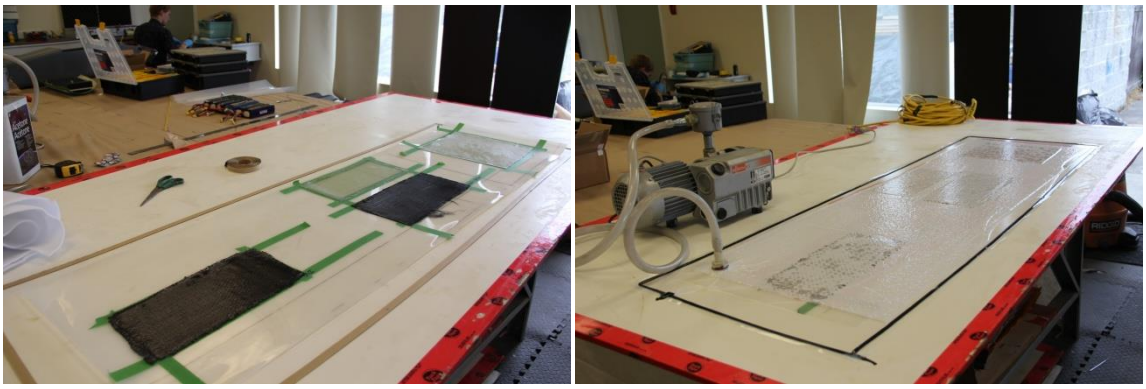

Figure 2.13 - Lamination of the rectangular shape of coupons (left) and the vacuum bag (right)

It was used the wet-layup process, in order to reproduce the same situation that was used to create the scale RPV. After the 24h of the vacuum process, the epoxy was cured and the excess of material in the rectangular shape was cut using a drill. The next step is to sand the zone where the glass fibre tabs were glued as shows Figure 2.14. It was used a pencil mines of 0.5mm to give the exact height of the adhesive which is in agreement with the regulations.

Figure 2.14 - Adhesive of fibre glass tabs in the rectangular shape

When the tabs where cured, the rectangular shape were cut by a water-jet machine, and finally the cut faces were sanded to remove any stress peaks. Before doing the tensile test, the width

and the thickness along the length of the coupons were measured. These values are in ANNEX A. All coupons produced can be seen in Figure 2.15

Figure 2.15 - Test specimens, carbon fibre woven (left), carbon fibre uni-directional (mid), glass fibre woven (right)

To test the coupons (Figure 2.16) it was used the document ASTM D3039/D 3039 M - 08 “Standard test method for tensile properties of polymer matrix composite”.

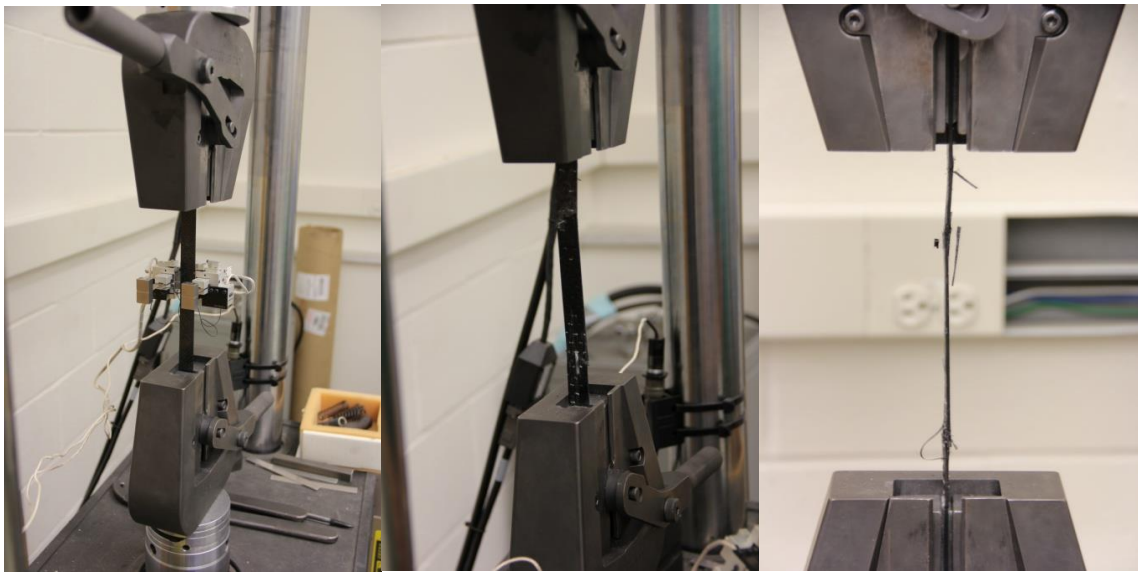

Figure 2.16 - Tensile Tests at different angles

After the tensile tests were done, the results were worked in order to get the Young Modulus and the Poisson’s ratio. It was conclude, that there was some slip between the fiberglass tabs and the clamps of the machine, due to this fact, the results were not realistic and so they are not documented in this thesis.

However sensitivity studies where preformed, to demonstrate the influence of each material property in the FEA results. Using the last project (Figure 2.10) and only the step3 (Figure 2.11) to performed this sensitivity study. The material properties, Young modulus, Poisson’s ratio and shear module were added as design variables and the values for joints were fixed. In this sensitivity study only the material properties can vary within a 10% margin from their original values.

The influence can be seen in the tornado diagram (Figure 2.17).

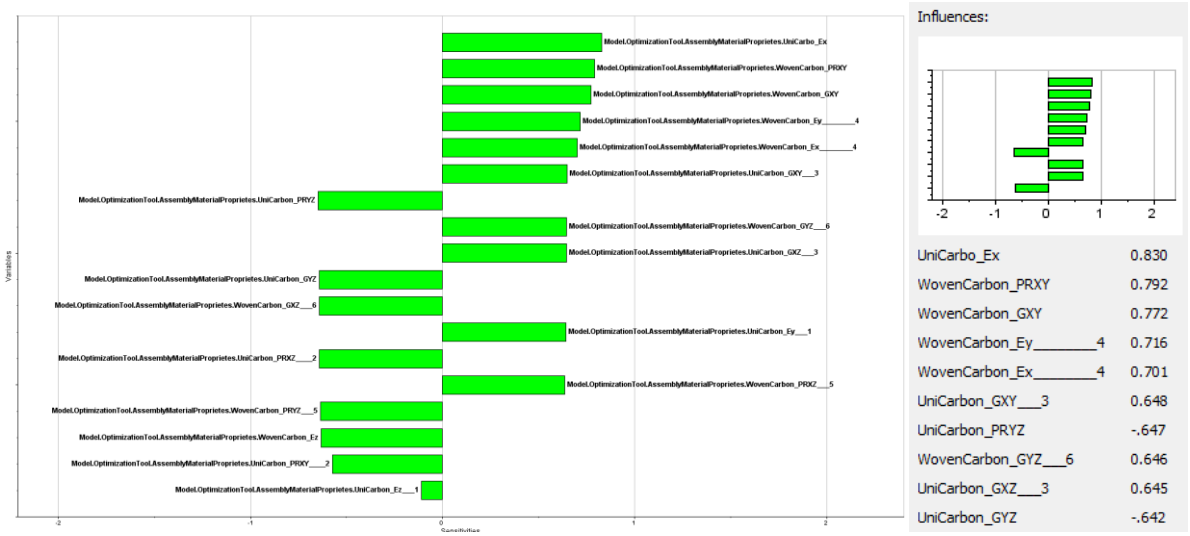

Figure 2.17 - Sensitivity study of the material properties for Carbon Fiber Woven and Unidirectional

This study reveals a huge influence of the material properties on the response of the problem.

The property that has the highest influence was the Young modulus of the unidirectional carbon fibre, as this material is the strongest one. The Poisson's ratio and shear modulus of the woven carbon fiberr were observed to have an impact on the results, which was not expected.

3. Simplified Beam model in ANSYS™

ANSYS™ is a finite element program, which in this thesis will be used to run the FEM. Next a brief theoretical background about elements and analysis type used in this project is presented.

3.1. Element BEAM188

BEAM188 is suitable for analysing slender to moderately thick beam structures. The element is based on Timoshenko beam theory which includes shear-deformation effects [20].

The element is a 3D linear, quadratic, or cubic two-node beam element. BEAM188 has six degrees of freedom at each node. These include translations in the x, y, and z directions and rotations about the x, y, and z directions. This element is well-suited for linear, large rotation, and/or large strain nonlinear applications [20].

Timoshenko beam theory, which is a first-order shear-deformation theory: transverse-shear strain is constant through the cross-section (*i.e.*, cross-sections remain plane and undistorted after deformation) [21].

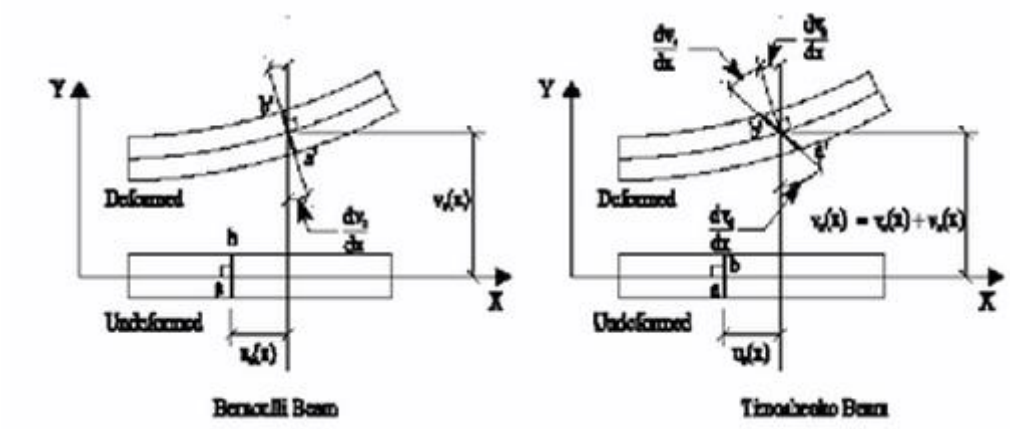

Figure 3.1 - Bernoulli Beam vs Timoshenko Beam [21]

The element can be used for slender or stout beams. Due to the limitations of first-order shear-deformation theory, slender to moderately thick beams can be analysed. The stiffness matrix of this beam element is:

$$\bar{\mathbf{K}}_e = \begin{bmatrix} \frac{EA}{L} & 0 & 0 & -\frac{EA}{L} & 0 & 0 \\ & \frac{12}{1+\Phi}\frac{EI}{L^3} & \frac{6}{1+\Phi}\frac{EI}{L^2} & 0 & -\frac{12}{1+\Phi}\frac{EI}{L^3} & \frac{6}{1+\Phi}\frac{EI}{L^2} \\ & & \frac{4+\Phi}{1+\Phi}\frac{EI}{L} & 0 & -\frac{6}{1+\Phi}\frac{EI}{L^2} & \frac{2-\Phi}{1+\Phi}\frac{EI}{L} \\ & & & \frac{EA}{L} & 0 & 0 \\ & \text{SYM} & & & \frac{12}{1+\Phi}\frac{EI}{L^3} & -\frac{6}{1+\Phi}\frac{EI}{L^2} \\ & & & & & \frac{4+\Phi}{1+\Phi}\frac{EI}{L} \end{bmatrix}$$

Figure 3.2 - Stiffness matrix of the Thimoskenko beam element [21]

3.2. Element MPC184

MPC184 comprises a general class of multipoint constraint elements that apply kinematic constraints between nodes. The elements are loosely classified here as “constraint elements” (rigid link, rigid beam, *etc.*) and “joint elements” (revolute, universal, *etc.*). The constraint may be as simple as setting the displacements equal between nodes. The rigid part of the structure may be modelled with the MPC184 link/beam elements, while the moving parts may be connected with any of the MPC184 joint elements [20].

The kinematic constraints are imposed by using one of the following two methods:

- The direct elimination method, wherein the kinematic constraints are imposed by internally generated constraint equations. The degrees of freedom of a dependent node in the equations are eliminated in favor of an independent node. The direct elimination method should be used whenever it is available since the degrees of freedom at the dependent nodes are eliminated, thereby reducing the problem size and solution time.

- The Lagrange multiplier method, wherein the kinematic constraints are imposed using Lagrange multipliers. In this case, all the participating degrees of freedom are retained. The Lagrange multiplier method should be used when the direct elimination method is not available or not suitable for the analysis purposes.

The disadvantage of the Lagrange multiplier method is that the Lagrange multipliers are additional solution variables and, hence, the problem size and solution time become larger when compared with the direct elimination method.

In this thesis, the Lagrange multiplier method is the only appropriate method to use due the existence of joints.

3.3. Geometry

The geometry of the Joined Wing aircraft has been converted into a simplified beam model. Using just points on the leading edge and steam chords from one spread sheet that Jenner Richard gave me access (ANNEX B). With this data, it was possible to create a 3D sketch in a commercial program (SolidWorks^{TM}) to have the exact coordinates of the points that are being implemented in a simplified beam model, which is showed in Figure 3.3 .

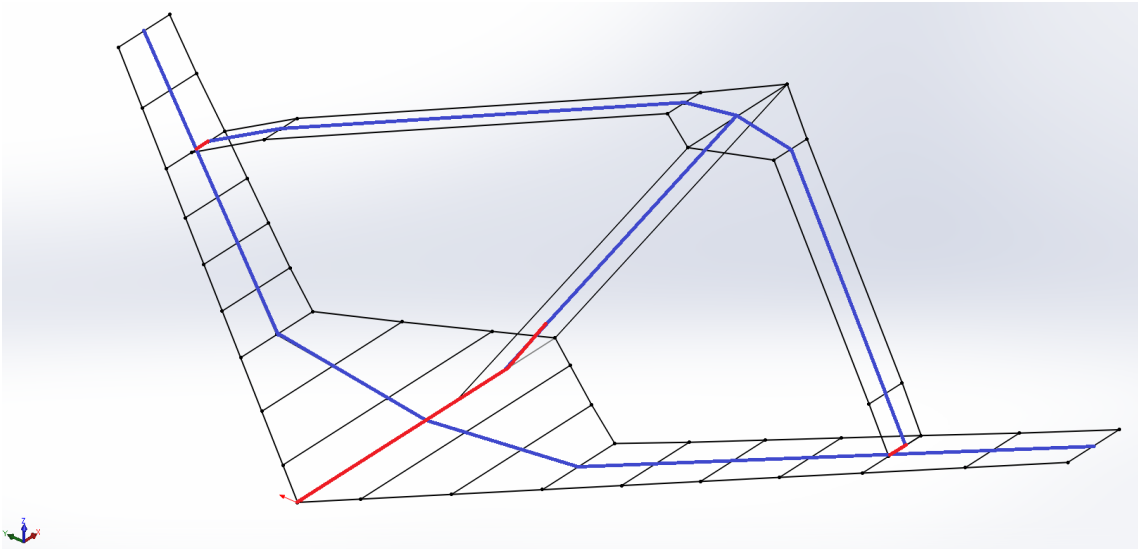

Figure 3.3 - Geometry of the Simplified Beam model

The blue lines are beams, which the points are in 50% of the chord along the span. So, this geometry is very similar to Sensorcraft. As we can see in the above figure, there is a line in the middle of the fuselage which it is a different element type. The red lines are rigid elements (MPC184), and they just transfer forces between nodes that are connected to it, creating moments that will be transferred to beams. These rigid elements are connecting the fuselage with joint on the boom, and are extend to the nose of the air plane in order to think in future. It will be possible to add mass points and match mode shapes after changing this mass points as Frederico did in [5]

In my first approach, the fuselage was very simplified, as nillustrated in Figure 3.4 . There are some lines connecting the front wing with the nose and boom. I did it this way because, I thought that the fuselage is the part from the airplane that has less influence on the results, but a small deflection on the fuselage will create a huge deflection on the wing tip.

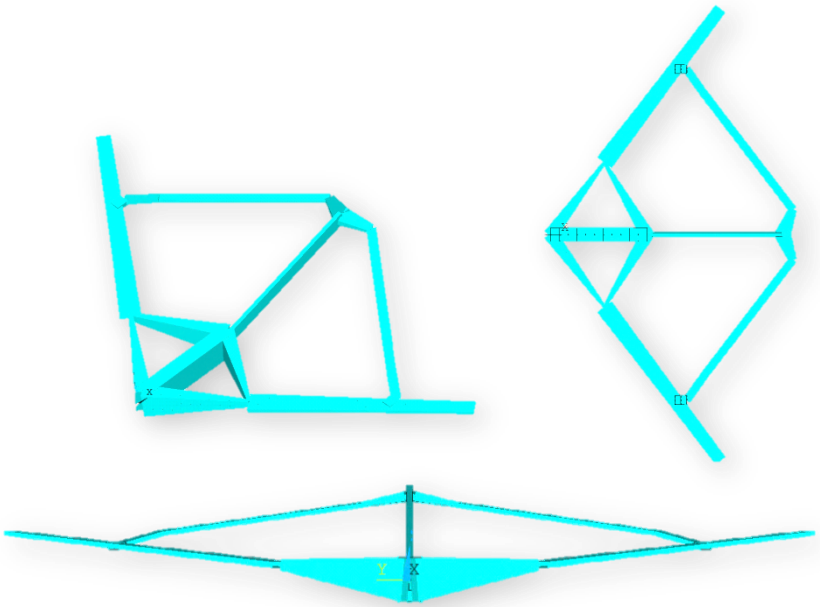

Figure 3.4 - First beam model

But I was wrong. So, after some results, I decided to make a much more realistic model as can be seen in Figure 3.5 .

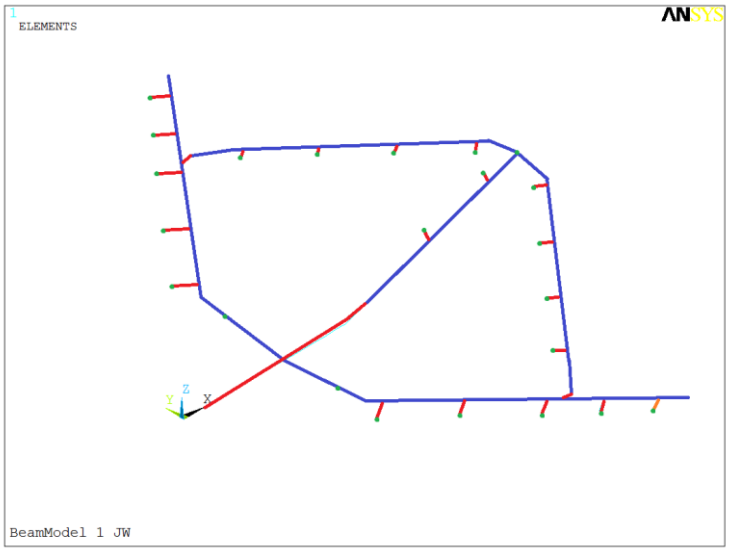

Figure 3.5 - Beam Model with rigid element to transfer the force at 0% of chord

There is a beam connecting the forward and rear wings. First, this beam is just a parallelepiped with a square base made of aluminium alloy, but in reality there are two pieces connecting the wings, which are made of the same material. In this case, this beam can bend and create a completely different response that expected. Creating another rigid element (MPC184) to transfer the forces between wings, can repair this problem. And so, in this case the deformation of airplane will not change due to the bending of this connection.

This model, as we already know, will be used to match the deformation of High Fidelity Model and experimental tests. The forces for this test will be applied in chord percentage in the ribs. So, to apply these forces in the same location, two keypoints were created, one at 0% and other at 100% of the chord. And then, a node between these keypoints is created using one variable called the $Ratio_K$, which is defined by:

$$Ratio_K = \frac{distance\ of\ node\ to\ leading\ edge}{chord\ of\ airfoil\ steam} \quad (2)$$

Forces will be applied at this node and the forces and moments will be transfer to the structure by a rigid element, MPC184. Therefore, the need to calculate, every time, the moments that should pass to the wing due to the translation of load points are not needed.

There will be 10 different load points in the forward wing, 8 points in the rear wing and 2 points in the boom. The possibility of simulating manoeuvres, with unsymmetrical loads cases, is the reason to create a full model and not just half of it. Figure 3.5 shows how this model looks like with these elements in 0% of the chord, in the leading edge of Sensorcraft. The green dots represent the load points.

The coordinates of the keypoints to create the simplified beam model in ANSYS™ can be seen in ANNEX B (points from SolidWorks™).

3.4. Joints

To join the parts of the model: fuselage, front wing, rear wing and boom; I decided to create universal joints. These joints on ANSYS™ can be model by the element MPC184 and with an unusual option activated. This kind of element connects two nodes which need to be on the exact same coordinates. In this model we have 4 different joints, connecting the fuselage with the forward wing, fuselage and boom, boom and strake, and finally forward wing and rear wing. The referential of these elements can be seen in Figure 3.6 which they link the parts of the airplane, the fuselage is link to the front wing (ref. 15 and 16) and to the boom (ref 11), the boom link to the strake (ref 12), and finally both wings are linked to other (ref 13 and 14).

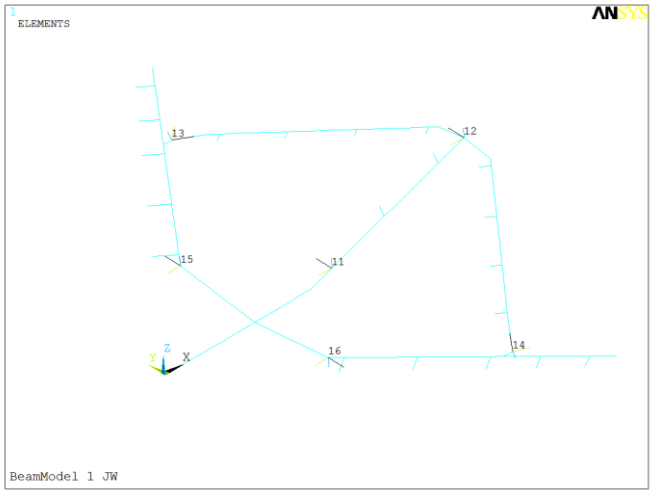

Figure 3.6 - Beam Model and the numbering of the Joints referential

The stiffness of the joints is a 6x6 matrix. The terms are coupled, which means that the terms at off-diagonal are 0, and the first 3 terms are corresponding to the spring stiffness in translation xx, yy and zz axis which are very high (the magnitude order is 10^9). And then we can model the last 3 terms at the diagonal that are the rotation along xx, yy and zz axis. I assume that there is just one axis about which the joint can rotate. As we can see, Figure 3.7 shows the axis where the joints can rotate, like a torsion spring.

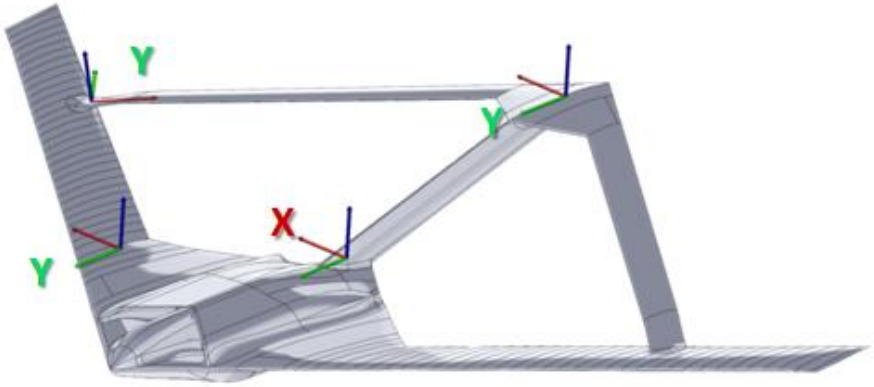

Figure 3.7 - Original CAD model with the allowable joints rotations

3.5. Section properties

Beams were model with hollow sections which, as a start point the base and height were set equal to 60% of chord and thicknesses, respectively, of the airfoil. To separate moments of inertia and torsion constant, I decided to have two different thicknesses, the bottom and top caps are equal and the left and right webs are equal too. Changing the wall thicknesses of the box we are changing the stiffness of the section for bending and torsion. Also changing the base and height will create different MOI and J. The wings and fuselage are modelled as tapered beams to account for the changes in stiffness along these components' length.

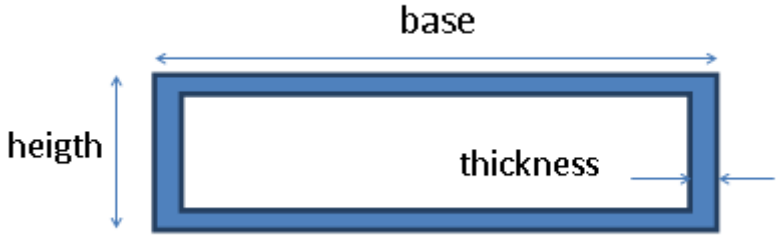

Figure 3.8 - Hollow Cross Section

Another variable was the TAPER which is defined below.

Thickness vs Length:

$$a = thickness_{root}$$

$$b = thickness_{tip} = TAPER \times a$$

Eq. 1: $y_1 = \left(\frac{y_B - y_A}{x_B - x_A}\right) x + y_A$

Eq. 2: $y_2 = \left(\frac{y_{B'} - y_{A'}}{x_B - x_A}\right) x + y_{A'}$; $where\ y_{A'} = y_A - a$; $y_{B'} = y_B - b = y_B - TAPER \times a$

The thickness along forward wing is equal:

$$t(x) = y_1 - y_2 = a\left[\frac{TAPER - 1}{x_B - x_A} x + 1\right] \quad (3)$$

To get closer to the reality, it was added twist to the beams, because the wings of the airplane have twist too. So, to know the twist angle I use all the geometry points that I have access and, after using a cubic spline, it is possible to know which angle will be implemented in the beam model.

3.6. Area moment of inertia

The area moment of inertia or second moment of inertia (I) is a term used to describe the capacity of a cross-section to resist bending. It is always considered in respect to a reference axis such as X-X or Y-Y. It is a mathematical property of a section concerned with a surface area and how that area is distributed along the reference axis (axis of interest). The reference axis is usually a centroid axis.

The moment of inertia is expressed mathematically as:

$$I_x = \int Ay^2 \, dA \quad (4)$$

$$I_y = \int Ax^2 \, dA \quad (5)$$

Where:

y = distance from the x axis to area dA

x = distance from the y axis to area dA

3.7. Polar Moment of Inertia

The polar moment of inertia is a quantity to estimate the resistance to angular torsion. It is a geometrical property of a cross section. Physically, it is a measure of how difficult it is to turn a cross-section about an axis perpendicular to it (the inherent rotational stiffness of the cross-section).

The polar moment of inertia is expressed mathematically as:

$$J = \int A(x^2 + y^2) \, dA = I_x + I_y \quad (6)$$

Finally for a hallow beam the MOI about yy axis and the J are:

$$I_{yy} = \frac{1}{12}[tb^3 - t(b-2t)^3] \tag{7}$$

$$J = \frac{2t_1 t_2 (b-t_1)^2 (h-t_2)^2}{bt_1 - ht_2 - {t_1}^2 - {t_2}^2} \tag{8}$$

3.8. Material properties

In order not to have so many variables, an isotropic material was chosen for the entire model. All beams are model of aluminium alloy. The properties for this material are:

Density=2800Kg/m3

Young Modulus=70GPa

Poisson's Ratio=0.35

In this project, the numbers for the material properties do not need to be realistic. This simplified beam model is just a mathematical model and not a model that could be built.

3.9. Forces

The forces that we will use are loads on the connections between both wings and on the top of the boom. On wings the load is positive in the zz direction, and on the boom the load is negative in the zz direction.

3.10. Analysis

The first analysis type will be linear static, and the objective is to reach the values of the 3.5g manoeuvre load case. After, non-linear analysis will be run in order to understand the behaviour of the structure in relation to with the variation of some variables. For the non-linear analysis, it will not be use the follower forces, which are forces that change the direction such that they stay always perpendicular to the line where is applied on all the load steps.

Sensitivity analysis and also carpet plots will be made for both types of analysis.

The time to perform a analysis on the high fidelity model compared with the beam model is 60 times higher. That is the reason to use a simplified model to understand the design space of this kind of joined wing configuration.

4. Computation Tool – ModelCenter™

4.1. Introduction of ModelCenter™

ModelCenter™ is an innovative software product from Phoenix Integration™, which is located in the Virginia Tech Corporate Research Center. Phoenix Integration was started by two Virginia Tech doctoral students, Scott Woyak and Brett Malone, the first one working in software integration of CAD program created by IBM™ and the second one doing research on computer-aided aircraft design for NASA in the ACSYNT (AirCraft SYNthesis) Institute. The two teamed up with Arvid Myklebust, a professor of mechanical engineering, to found Phoenix™ in 1995 [22].

This program has the ability to perform distributed modelling and analysis in order to provide design and manufacturing tools for engineers [23]. This software provides the user with a unique way of "wrapping" other computational cods or software's. Warp is the termed used when program codes, originally conceived to be operated in a "stand alone" manner, can communicate with each other directly. It uses a unique architecture to wrap and integrate legacy programs, data, and geometry features. With this program it is possible to perform different studies as the performance of parametric and optimization studies, Design of Experiments (DoE), Response Surface Methodology (RSM) and the ability to save, track and compare design histories [23]. So, ModelCenter™ can save time in the project by coordinating multiple engineering programs to be linked between each other [24].

For this project, different programs were integrated in ModelCenter™ :

- ANSYS™ – is a finite element commercial code for numerically solving a wide variety of mechanical problems [25]. In this thesis, this software was used to perform linear and non-linear static finite element analyses.
- MatLab™ - is a high-level language and interactive environment for numerical computation, visualization and programming [26]. It was used to create and output plots for each optimization run.
- VBScript - short for *Visual Basic Scripting Edition* is a scripting language developed by Microsoft™. VBScript is based on the Visual Basic programming language, but it is much simpler [27]. It is used to link variables and to do calculations.
- Excel - is a spread sheet program created by Microsoft™ and it is included in the package of Office. This program allows users to input numerical values or data into rows or columns of a spread sheet, and to use these numerical entries for different things as calculations, graphs, and statistical analysis [28].

There are many benefits from using ModelCenter™ as: decreasing the design time, more design alternatives can be explored, improved understanding of the design space, fewer errors between different departments, archiving the design information.

4.2. Description of the project

As it was said before, ModelCenter™ can integrate different programs in the same project. Figure 4.1 shows the overview of this project. In the next sub chapters, the modules will be described to explain how the project flows.

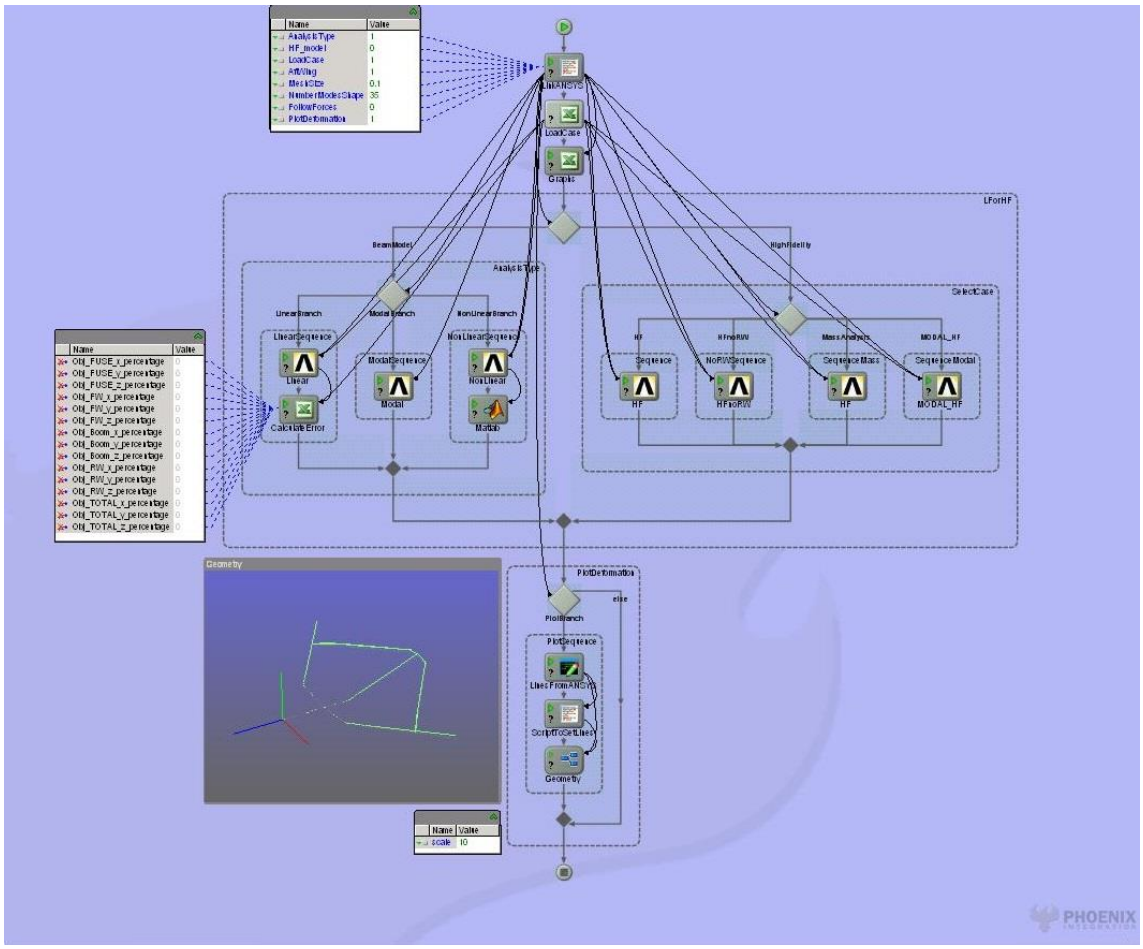

Figure 4.1 - Overview of the Project in ModelCenter

4.2.1. Variables in VBscript

This project starts with a pre-processing VBscript, which creates the ModelCenter™ variables and links to ANSYS™, branch if-cases and ANSYS™ input. This script has the entire variables used and they are for analysis control:

- **AnalysisType –** it is used inside the ANSYS™ script to tell the program which analysis show be done. Choose the path for the project (1-Static; 2-Modal; 3-Non-linear)
- **HF model –** choose the path for project (0-goes to the Beam Model, left side; 1-goes to the High Fidelity Model, right side)
- **Loadcase -** if the analysis is static linear or non-linear, then the user must specify which load case wants to run. The loads are inside the first excel input named “Load Case”, and it will be described in another section.

- **AftWing –** decide if the model has the aft wings or not (1 if the aft wings are to be considered and 0 if not)
- **MeshSize –** input value for the length of finite elements
- **Number of Modes Shape –** it is only used when running a modal analysis and as its name says, chooses the number of the first nth modes shapes to be computed.
- **FollowForces –** it is used when the analysis is non-linear to decide if follower forces or constant forces are used.
- **PlotDeformation –** is a flag to update the deformation plot for each run when on during optimization, this flag should always be off, to gain around 5 seconds for each run.

For the finite element Beam Model, the variables are:

- **Cross section properties**: base, height, thickness of the bottom/top caps and left/right webs;
- **Material properties**: Young modulus, Poisson's ratio, density;
- **Mass Points**: masses on each node;
- **Joints Values:** Fuse-FW, Fuse-Boom, Boom-RW and FW-RW joint values;

Finally, for the High Fidelity Model the variables are the material properties for all the fibres properties, woven, unidirectional and isotropic material as aluminium, gelcoat and sanfoan. It was included the joints as variables as well.

4.2.2. Loadcases-spreedsheet

The name of each load case and the points/magnitudes are summarized in Table 4.1. These loads are not aerodynamic loads, they are just values selected to match both models.

Name of Load case	Fuse Load Without Aft Wing	Boom Load Without Aft Wing	Forward Wing Load Without Aft Wing	Full Wings
Load case number	**1**	**2**	**3**	**4**
FORCE FUSE [N]	200	0	0	0
FORCE FW1 [N]	0	0	100	100
FORCE FW2 [N]	0	0	100	100
FORCE FW3 [N]	0	0	100	100
FORCE FW4 [N]	0	0	100	100
FORCE FW5 [N]	0	0	100	100
FORCE BOOM1 [N]	0	100	0	0
FORCE BOOM2 [N]	0	200	0	0
FORCE AW1 [N]	0	0	0	100
FORCE AW2 [N]	0	0	0	100
FORCE AW3 [N]	0	0	0	100
FORCE AW4 [N]	0	0	0	100

Table 4.1 - Summary of the Load cases

The ratio of point load is the chord wise position of the point as defined in equation 2.

Table 4.2 shows the ratio for each load case. Briefly, all load cases have a 0.5 in ratio, *i.e.*, the centroid of beams. This value was chosen to simplify the application of loads and the interpretation of results.

Name of Load case	Fuse Load Without Aft Wing	Boom Load Without Aft Wing	Forward Wing Load Without Aft Wing	Full Wings
Load case number	**1**	**2**	**3**	**4**
Ratio FW1	0.5	0.5	0.5	0.5
Ratio FW2	0.5	0.5	0.5	0.5
Ratio FW3	0.5	0.5	0.5	0.5
Ratio FW4	0.5	0.5	0.5	0.5
Ratio FW5	0.5	0.5	0.5	0.5
Ratio AW1	0.5	0.5	0.5	0.5
Ratio AW2	0.5	0.5	0.5	0.5
Ratio AW3	0.5	0.5	0.5	0.5
Ratio AW4	0.5	0.5	0.5	0.5

Table 4.2 - Ratio of the Point Load for all Load cases

In the next figures (4.2 – 4.4) are illustrated the application points for each load case. The points are located in the Sensorcraft spars.

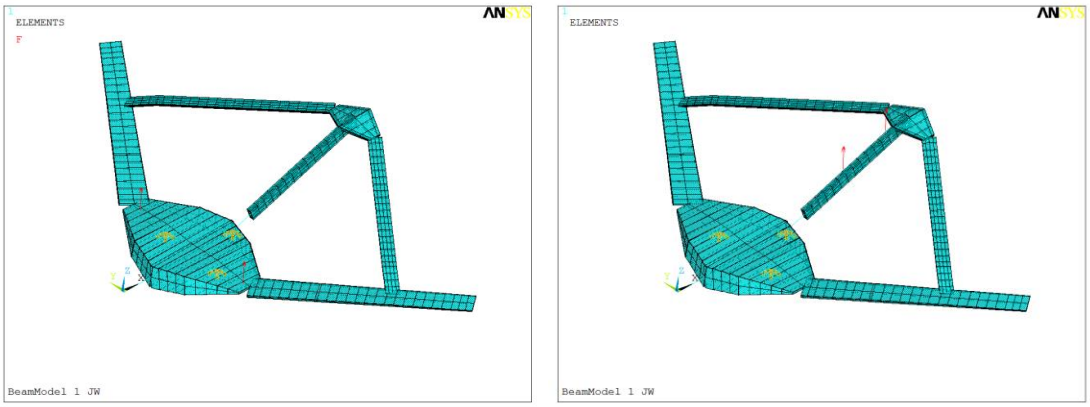

Figure 4.2 – Beam model Fuse Load (left) and Boom Load (right)

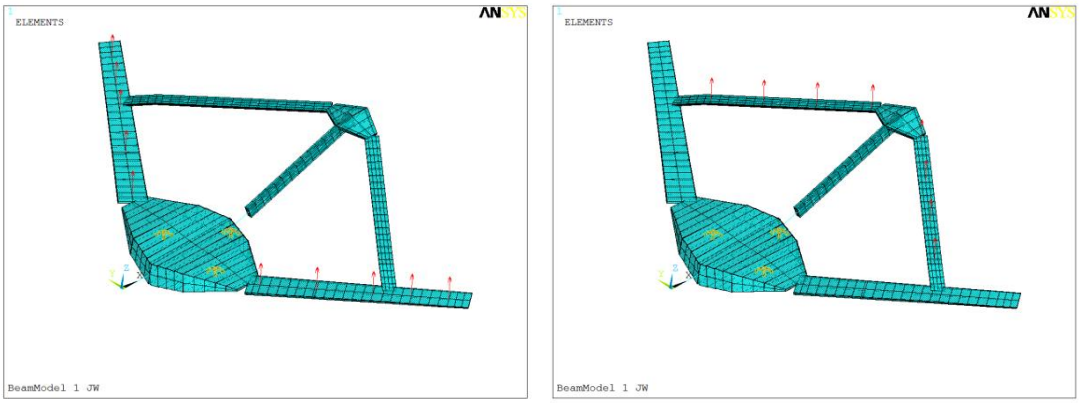

Figure 4.3 – Beam Model Forward Wing Load (left) and Aft Wing Load (right)

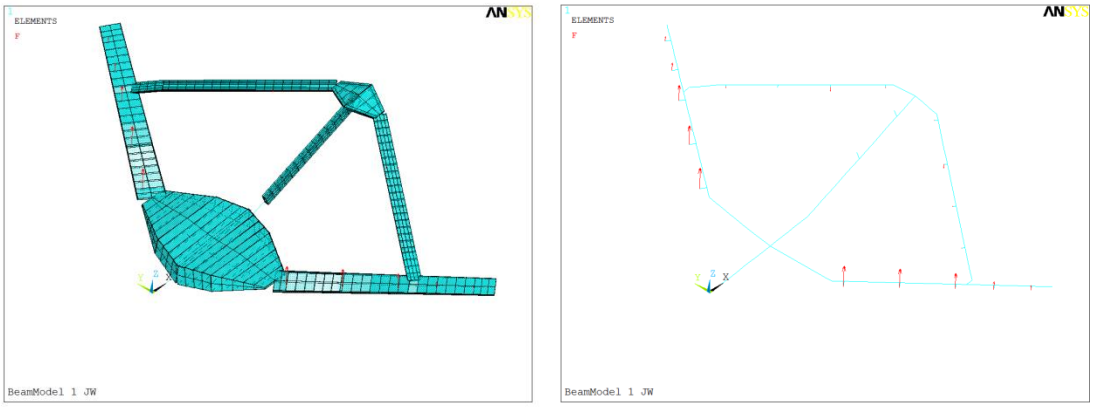

Figure 4.4 – Beam Model Full Wings Load (left - beams shape; right– 1D elements)

If the idea is to match the aircraft in just one load case, the optimization will result in design variables that could not be compatible with other load cases. The numbers of variables will make the optimization a huge computational problem. To avoid this option, it was created one load case to match the Fuse, then the Boom and finally the Forward Wing, fixing the variables for these parts. In the end, one last load case was optimized changing only the variables for Rear Wings. With this idea in mind, the optimizations process becomes simpler because, the number of variables will be less than with just one full optimization.

4.2.3. Graphs-spread sheet

Due to the large number of FW variables, this spread sheet as used as debug. Inside it, one can see the base and height of the cross sections, Young modulus, MOI and J which varies allow the span.

Next series' graphs show the different aspects of these variables. To understand how these variables work together, it was changed all the variables for FW and plots were inside in the same graph, which can be seen below.

Dotes on graphs in Figure 4.5 and 4.6 e the midpoints of each beam.

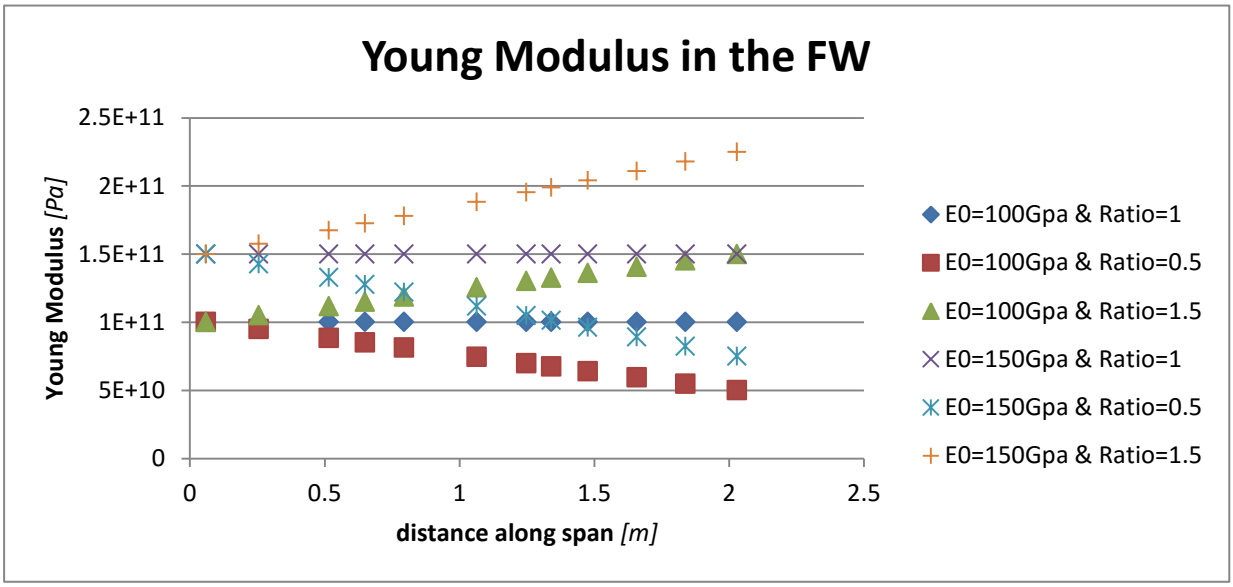

Figure 4.5 - Young Modulus along the span of the Forward Wing changing E0 and Ratio

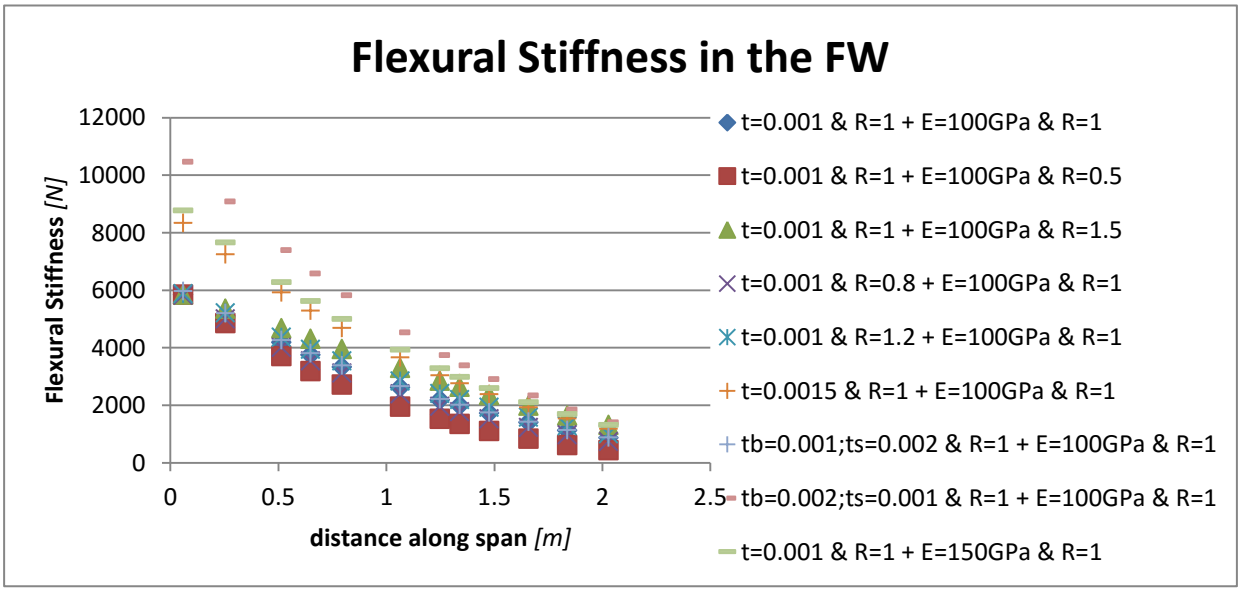

Figure 4.6 - Stiffness along the span in the Forward Wing

In the next graphs, dotes are in the end points of the beams with different cross section. For example, the first beam was 2 different cross sections (first and second dot); the first cross section of the second beam is the same of the second cross section of the first beam, and so on.

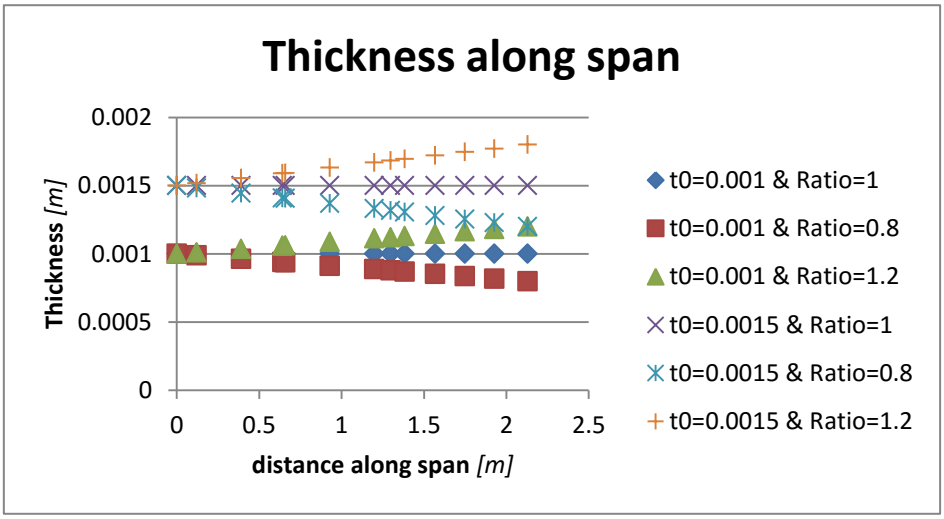

Figure 4.7 - Thickness Side along the span in the Forward Wing

Next the second MOI in yy axis and J are presented using the thickness and the taper ratio as variables.

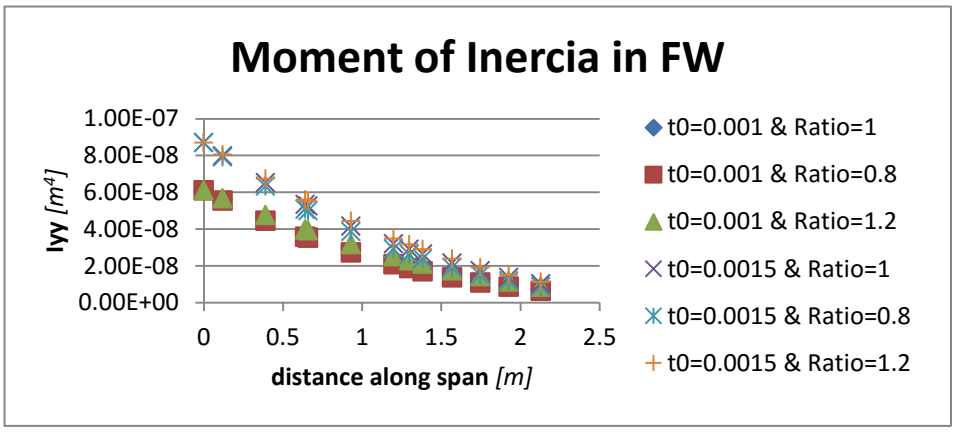

Figure 4.8 – Moment of Inertia along the span in the Forward Wing

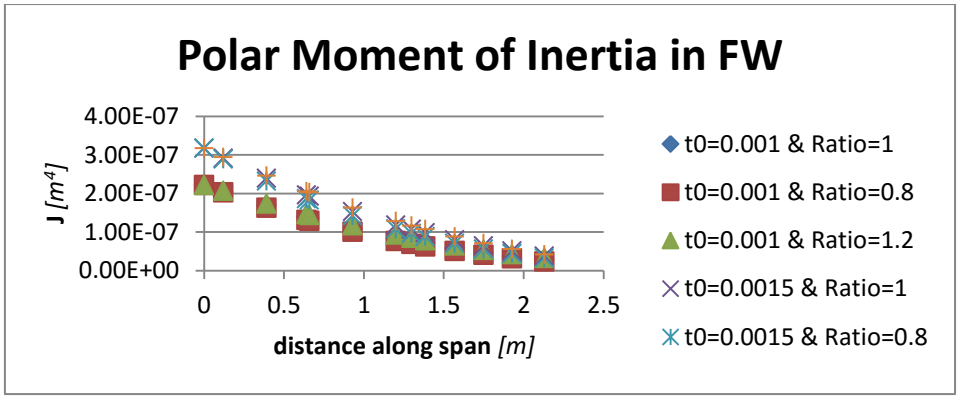

Figure 4.9 – Polar Moment of Inertia along the span in the Forward Wing

4.2.4. Calculate Error spread sheet

This spread sheet calculates all the errors required to compute the objective function to match the linear static response. The inputs are the displacements X, Y and Z at the nodes to match and the load case number. The outputs are the error in percentage for all the nodes measure, for different parts of the airplane (Fuse, FW, RW and Boom) and the overall error.

In this section are the results for the High Fidelity model for all load cases. Results for computing the load came for the right branch of the project, and then they are used in this excel file.

The first input is the load case number, which chooses which values are the targets. Then with the displacements from the FEA, the errors are calculated.

The objective functions are set as the sum of all the relative error to the power of two. In this way, error will never be negative. Each node has one objective function, so the optimization is multi objectives.

$$objective\ function = \left(\frac{value\ from\ FEM - target\ value}{target\ value}\right)^2 \tag{9}$$

The output of interest is the percentage error, which is simply the square of objective function times 100.

$$percentage\ error = \sqrt{objective\ function} * 100 \tag{10}$$

The average error of each part of the Sensorcraft, is the sum of all errors divided by the number of nodes to match. Next table show the number of nodes to match.

Part	Nº of nodes to match
Fuse	1
Boom	5
FW	10
RW	7
Total	23

Table 4.3 - Number of nodes to match for the different parts of the JWSC beam model

4.2.5. Non-linear calculations on MatLab™

This spread sheet was used when a non-linear analysis was needed, to understand the non-linearity's of the structure. In order to do so, some parameters were defined and calculated for each run.

Equation 11 was used to understand the stiffening or softening of the boom and a large nonlinear deformation due to load stepping.

$$NL\ Factor\ Boom = \frac{10(LinearSlopeBoom * haltime - DispBoom\ in\ ZZ(end))}{\max|DisplBoom|} \tag{11}$$

A parameter (see equation 12) was generated in order to check if the boom deflection reverses over the time history. The first term is only to find a negative sign if reversal occurs, the second term shows the magnitude of that reversal. So, the more negative is this parameter the higher reversal is.

$$Reverse\ Factor = \frac{\frac{DispBoom\ in\ ZZ(end)}{LinearSlopeBoom}}{abs\left(\frac{DispBoom\ in\ ZZ(end)}{LinearSlopeBoom}\right)} * abs(maxDisplBoom - minDisplBoom) \tag{12}$$

Another situation that could be found on the geometry of a diamond shape is the buckling of the rear wing. In order to verify this problem, a parameter was created (equation 13). This parameter checks if the rear wing curvature is far from the linear behaviour by comparing the distance of a midpoint node to a line connecting the two ends of the wing.

$$Buckling\ Factor = midNode_{RW} - (RW\ slope * 0.5 + rootNode_{RW}),$$
$$\text{Where: } RW\ slope = tipNode_{RW} - rootNode_{RW} \tag{13}$$

4.2.6. Algorithm used on the process

Darwin algorithm was the algorithm chosen to run this optimization.

Darwin is a genetic search algorithm developed specifically for solving engineering optimization problems It is able to effectively search non-linear and noisy design spaces. When more than one objectives are defined, Darwin will search for a series of best designs using non-dominated design search [23].

The Darwin algorithm ensures that the optimization procedure continually progresses towards an optimal solution by allowing the best designs in each generation to survive for the next generation with the cost of an enormous amount of runs [23].

4.3. Results of matching Beam Model with High Fidelity Model

After a long travel on this optimization process, there are the results of the matching the High Fidelity Model with a simplified Beam Model. Too many iterations, versions and ideas, but all resumes to this idea: on the static convergence, all the displacements in zz should be matched in different points of the structure.

The optimizer chosen was the Darwin algorithm and after 15000 runs, the best value found was in iteration 9701. The errors are described in Table 4.4 for the match nodes and also for the different parts of the JWSC in Table 4.5.

Error nº	%	Location
1	7.95	Fuse1
2	8.06	FW1
3	7.30	FW2
4	7.44	FW3
5	7.69	FW4
6	7.85	FW5
7	7.87	FW6
8	7.89	FW7
9	7.91	FW8
10	7.93	FW9
11	7.95	FW10
12	5.70	BOOM1
13	5.73	BOOM2
14	5.79	BOOM3
15	5.83	BOOM4
16	5.86	BOOM5
17	5.33	RW1
18	3.67	RW2
19	0.31	RW3
20	0.07	RW4
21	4.62	RW5
22	6.45	RW6
23	7.28	RW7

Table 4.4 – Errors of the Simplified Beam model relatively to the HF model at different nodes

Average Error on:	%
Fuse	7.95
FW	7.79
BOOM	5.78
RW	3.96

Table 4.5 – Average errors of the Simplified Beam model relatively to the HF model for the different aircraft parts

Overall, the error stays always below 8%. The discrepancy could be because the HF model has not symmetry results, and also due to very small displacements, in order of 10^{-5} , at some nodes. Nevertheless the results are acceptable, all errors are below 10%, and so this simplified model could

be used to perform several sensitivity studies and the DOE to understand the influence of some variables on the structure.

Finally, the results of the variables for this optimized point are represented in Table 4.6. To note that the N/A on the table means that the variable was not used in the optimization.

	Thickness (mm)		Tapper	Young Modulus (GPa)
	webs	caps		
FUSE	256.7	40.2	0.26	N/A
FW	69.2	1.1	0.77	N/A
RW	29.6	3.6	N/A	N/A
BOOM	17.8	40.5	N/A	480

Table 4.6 - Results of the variables used to match the HF model with the beam model

About the values in the previous table, the most important point to emphasize is that the Young Modulus of the boom is really high. This happens due to the fact that in the HF model this part of the structure is really stiff.

In the following subsections are presented the sensitivity studies for the beam model after matching the High Fidelity Model.

4.4. Sensitivity Study around the match point

Next, a series of sensitivity studies were performed on the joints and on the stiffness of the structural members in order to understand which parameters affect most the structural response.

The load case chosen is with the point loads applied at the joints with a magnitude chosen to yield equivalent forward wing root bending moments, of those of a 3.5g pull-up manoeuvre.

To perform the sensitivity studies, the variables can change within (±)10% from the initial value, which are previously optimized values.

In order to be easier to understand the next results, the reader should keep in mind the Figure 4.10, which shows the joints' variables and their respective colours in the results. The load case stays constant during the study and it was decided to use the point loads applied at the joints with the magnitude chosen to yield equivalent forward wing root bending moments of those of a 3.5g pull-up manoeuvre.

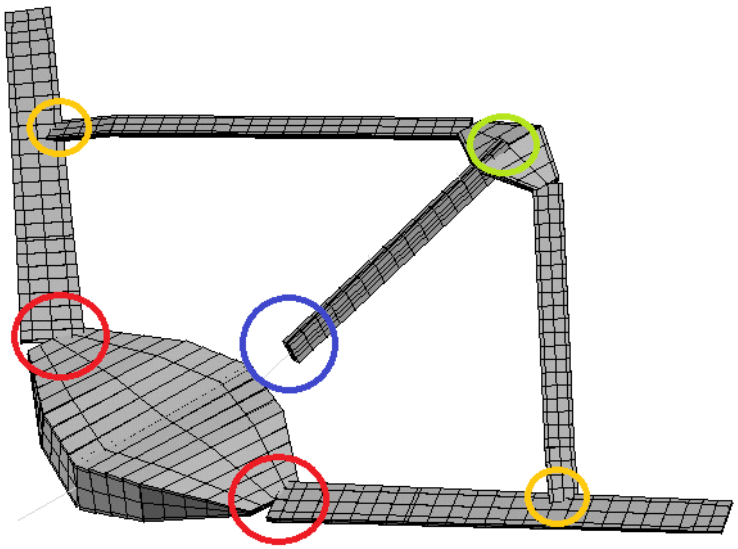

Figure 4.10 - Beam Model Joints' colour locations

Next are presented the sensitivity graphs of all joints variables with their respective colours. The bigger the bar is the more influence has that variable on the response. The responses are the boom deflection, wing deflection and also the ratio between the boom and the wing tip deflections. The deflections are only in the z direction.

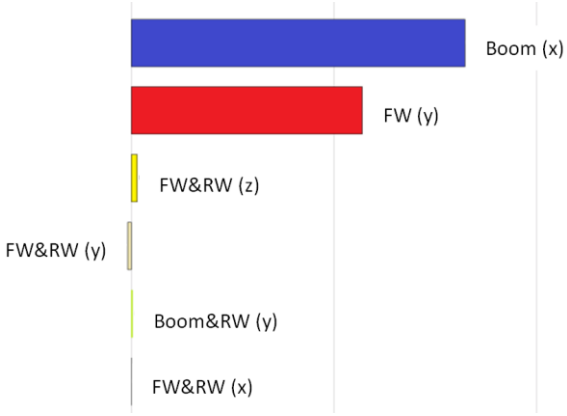

Figure 4.11 - Sensitivity Study for joints regarding boom deflection

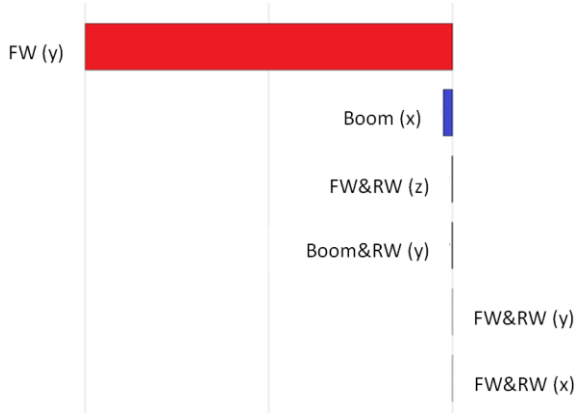

Figure 4.12 - Sensitivity Study for joints regarding wing tip deflection

Finally, in Figure 4.13, where the response is the ratio between wing tip and boom, the boom joint reveals to be the parameter that most influences the results. The wing deflection has also an impact in the response. The other joint variables will change the results, but not so much as the boom and forward wing.

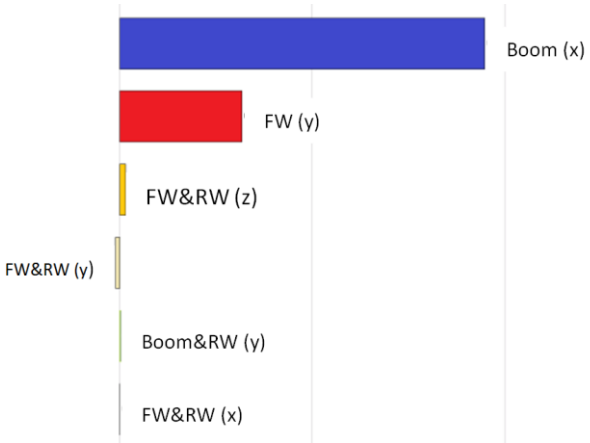

Figure 4.13 - Sensitivity Study for joints regarding ratio between boom and wing tip deflection

Similarly, an investigation into the effects of the running stiffness of the main structural components was performed. The load case is the same as before.

Also, the colours of the variables are described in Figure 4.14. Other variable rather than the thickness is the wing taper that reduce the thickness of the forward wing from the root to the tip.

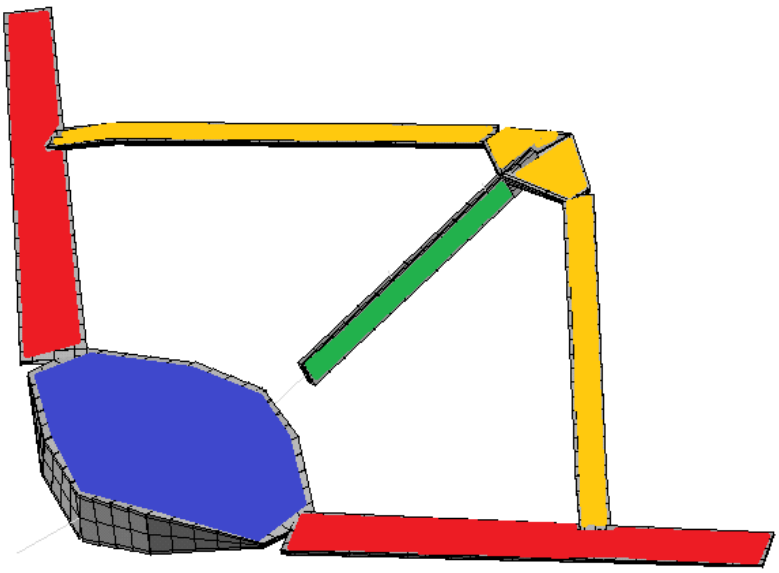

Figure 4.14 - Beam Model stiffness colour locations

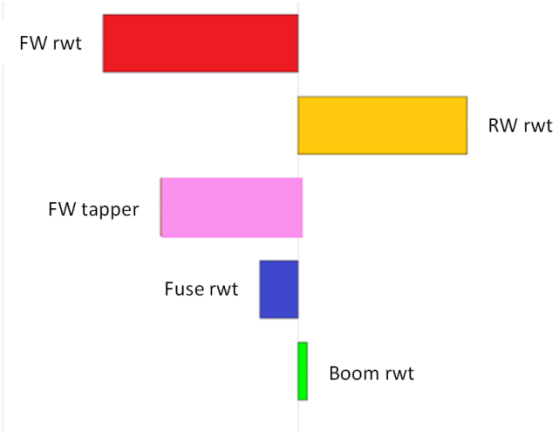

Figure 4.15 - Sensitivity Study for stiffness regarding boom deflection

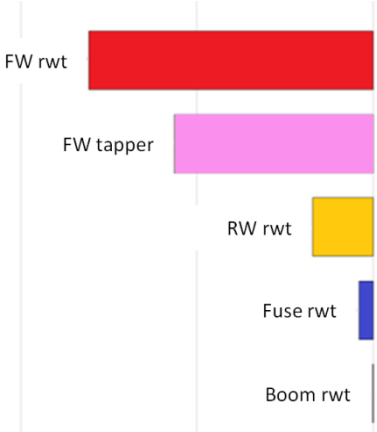

Figure 4.16 - Sensitivity Study for stiffness regarding wing deflection

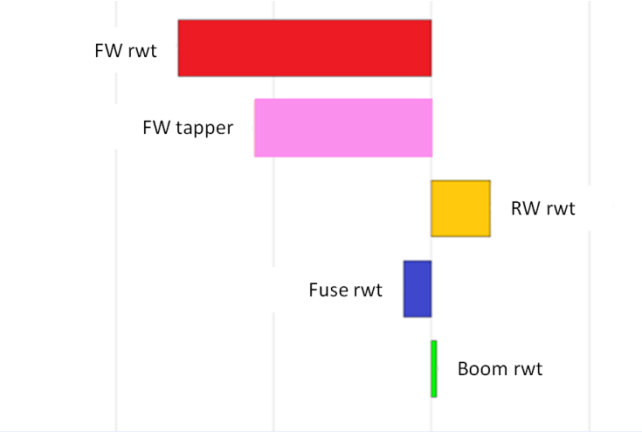

Figure 4.17 - Sensitivity Study for stiffness regarding ratio between boom and wing tip deflections

The thickness of the boom reveals to have a very small influence on the results. As expected the forward and rear wing are the parts of the structure that have the most influence on the results.

4.5. Design Space Exploration around the match point

With the DOE, it is possible to draw some carpet plots where each intersection between lines is one run of the simplified beam model. The response for the DOE is the ratio between boom and wing displacements.

The design space created for two joint variables has a dimension of 9x9, this means 81 runs. Only the FW(y) and Boom(x) joints were analysed as these variables were observed to have a higher influence on the response, as it can be seen in Figure 4.13. These variables can vary (±)100% their initial value. Table 4.7 shows the percentage of the joint variable in the carpet plot.

nº on the space	1	2	3	4	5	6	7	8	9
% change	-100%	-75%	-50%	-25%	0%	25%	50%	75%	100%

Table 4.7 – Percentage of variation of the joints in the carpet plot

Next is presented the carpet plot generated in the DOE study. The arrows in the next figures represent an increase of the corresponding variable in that direction.

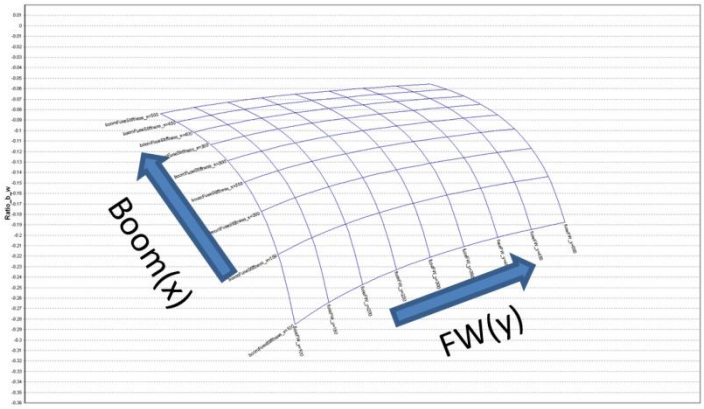

Figure 4.18 – Carpet plot of the FW(y) and Boom(x) joints with the response of the ratio between boom and FW deflections

From figure 4.19 it is possible to see that the gradient of the variable Boom(x) decrease when the FW(y) increase its value.

Next in this study, ratio wall thickness variables, for the FW, RW and Boom can change their initial value to the double or the half of the initial values. These are the boundaries for the study variables. The initial value is the optimized point. The design space created has a dimension of 16x16, this means 256 runs for each combination of two variables. The number of combinations is equal to three, FW & RW, FW and Boom and finally RW & Boom. Table 4.8 shows the percentage of the variable change in the carpet plot.

Nº on the space	1	2	3	4	5	6	7	8
% change	-100%	-87.5%	-75%	-62.5%	-50%	-37.5%	-25%	-12.5%

Nº on the space	9	10	11	12	13	14	15	16
% change	12.5%	25%	37.5%	50%	62.5%	75%	87.5%	100%

Table 4.8 – Percentage of variation of the ratio wall thickness in carpet plot

Next are presented the carpet plot generated in the DOE study. The arrows on the next series of figures represent an increase of the corresponding variable in that direction. The blue is for no boom deflection, so below the blue line the boom has a negative deflection in z direction, and above the blue line the boom has a positive deflection in z direction, the same positive direction as the forward wing.

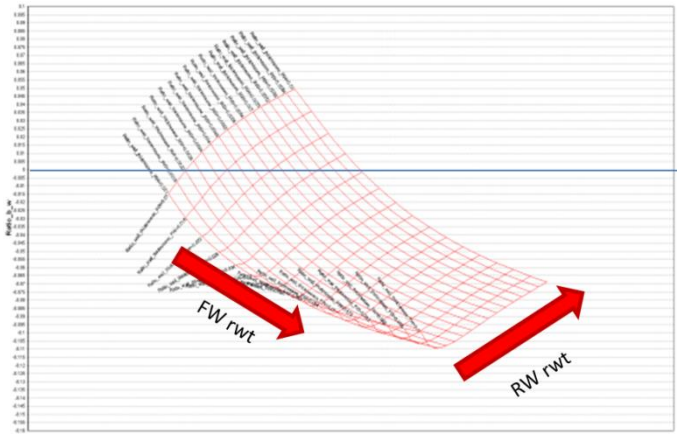

Figure 4.20 – Carpet plot of the FW and RW ratio wall thickness with the response of the ratio between boom and FW deflections

From Figure 4.20 it can be said that the combination of the stiffness of the FW and RW can cause the boom to goes up, instead of going down when the load is equivalent to the 3.5g manoeuvre. This can be possible with a lower stiffness on the FW and a higher value on the RW.

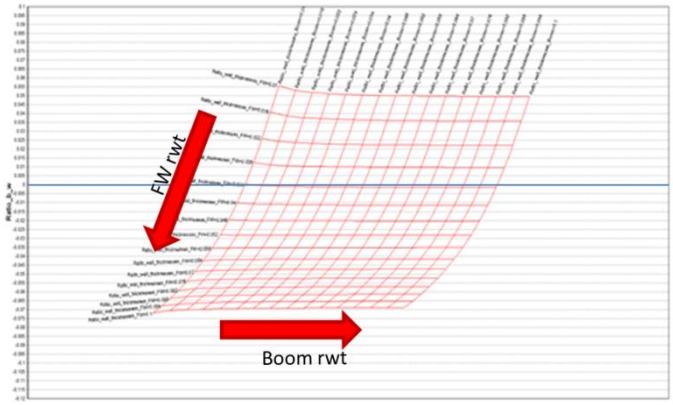

Figure 4.21 – Carpet plot of the FW and Boom ratio wall thickness with the response of the ratio between boom and FW deflections

Also, in Figure 4.21 it is possible to note that if the FW stiffness decreases 125% the boom will go up. The variation of the boom is not so relevant for this response. The very low value corresponds exactly to what was seen in Figure 4.15 - 4.17.

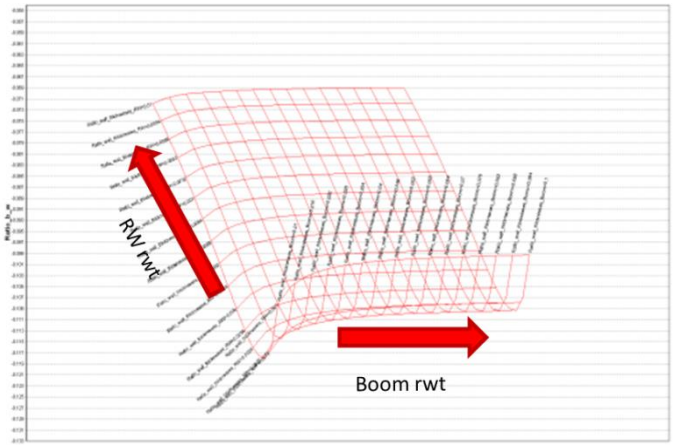

Figure 4.22 – Carpet plot of the RW and Boom ratio wall thickness with the response of the ratio between boom and FW deflections

From Figure 4.22 it can be concluded that by changing only the RW and the Boom stiffness it is not possible to make the boom going up.

4.6. Design Space Exploration of non-linearity's

Sensitivities of the nonlinear response were also investigated using the simplified beam model. Measures of nonlinearity were calculated for the boom as the NL Factor Boom and the Reverse Factor. An additional form of nonlinearity was investigated, the Buckling Factor of the RW. These parameters were already described, their meaning and how they are calculated, in subchapter "4.2.5 Non-linear calculations on MatLab".

The effects of both joint and structural stiffness were investigated.

In order to decrease the time of the analysis, as the non-linear takes much more time than a linear static, some variables were neglected. On non-linear analysis the solver updates the stiffness matrix on each load step and then it performs a linear static solver. This means, that if we have 10 time steps to solve, on each non-linear analysis, this will take at least the same time as the calculations solver of the 10 linear static analysis

The parameters, that were ignored, are the FW&RW(x) & FW&RW(z) due to the real joint showed very stiff on this degree of freedom. Also, the Fuse rwt and FW tapper were neglected, due to these parameters has a similar, but not on the same magnitude, as the FW rwt.

As before, to perform the sensitivity studies, the variables can changes +10% and -10% from the initial value, which are the optimized previous point.

The colour schemes stays the same as the linear study, Figure 4.10 and Figure 4.14 shows, respectively, the colours for the joints and for the ratio wall thickness variables.

The results for the joints are presented in images below, with the responses to be the NL Factor Boom, Reverse Factor and Buckling Factor for the Figure 4.23, Figure 4.24 and Figure 4.25, respectively.

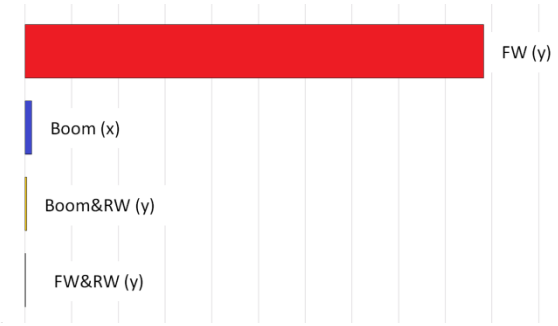

Figure 4.23 – NL Factor Boom: Non-linear Sensitivity Study for joints

Regarding this result, it could be said that stiffening or softening of the boom really depends of just FW(y) parameter.

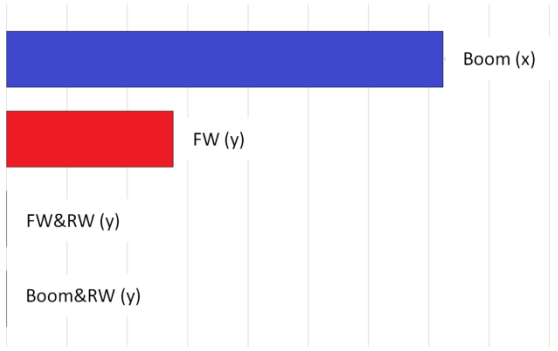

Figure 4.24 – Reverse Factor: Non-linear Sensitivity Study for joints

About the previous image, the change of the direction for the boom during the load increment depends mostly of the Boom(x), although FW(y) as also a significant influence on this behaviour.

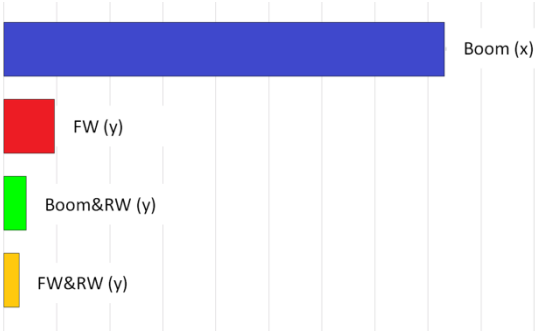

Figure 4.25 – Buckling Factor: Non-linear Sensitivity Study for joints

All variables cause an influence on the buckling of the RW, but the Boom(x) is the main driving parameter.

Next are presented the ratio wall thickness sensitivity study with the responses to be the NL Factor Boom, Reverse Factor and Buckling Factor in Figure 4.26, Figure 4.27 and Figure 4.28, respectively.

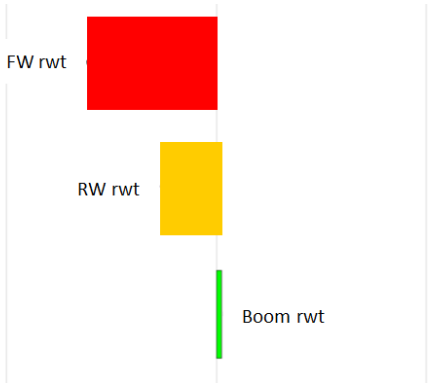

Figure 4.26 – NL Factor Boom: Non-linear Sensitivity Study for stiffness

Figure 4.27 – Reverse Factor: Non-linear Sensitivity Study for stiffness

From the previous two images, it is possible to conclude that the non-linearity's of the boom deepens mostly with the stiffness of both wings, instead of the stiffness of the boom itself.

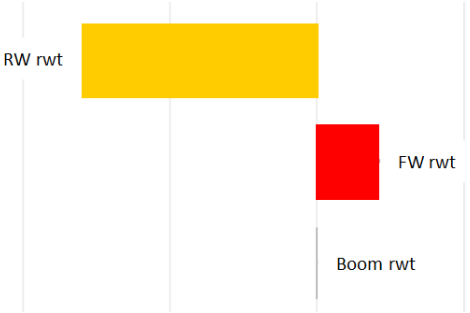

Figure 4.28 – Buckling Factor: Non-linear Sensitivity Study for stiffness

As expected the stiffness of the RW is the design driving parameter driver for its buckling.

A subset of the parameters with the largest effect on the nonlinear response was chosen to further investigate the design space. The parameter chosen was the FW and RW ratio wall thickness. A regular grid was used to build the Design of Experiments in order to explore the design space

Figure 4.29 shows the projection of the design space into three dimensions. With RW and FW stiffness in the plane, where the arrow shows the increase direction. The vertical axis shows a measure of the Non-Linear Factor.

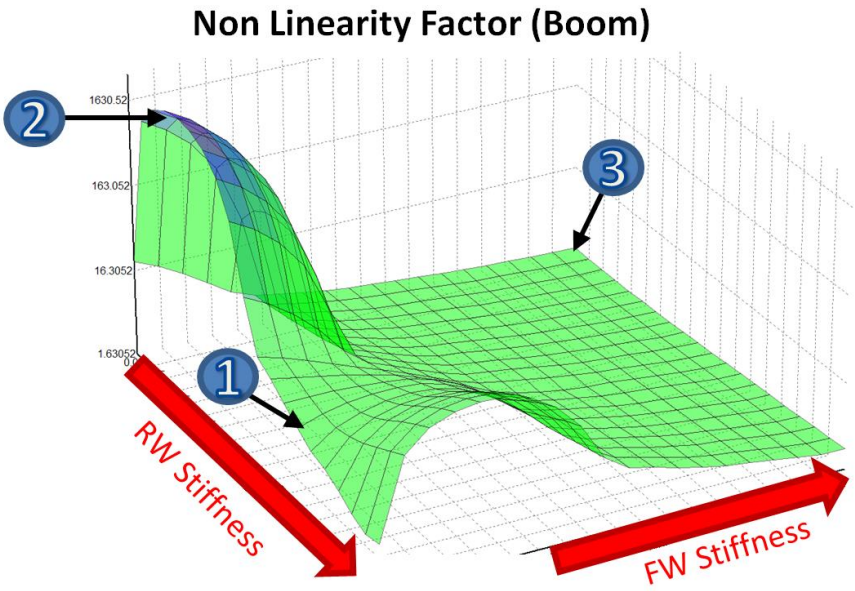

Figure 4.29 – Non-linearity Factor: design space

In this one slice of the design space we can see different forms of nonlinearity including the geometric stiffening of boom tip (1), the boom up/down reversal (2) and boom softening (3), where the deflections by the load steps can be seen on Figure 4.30.

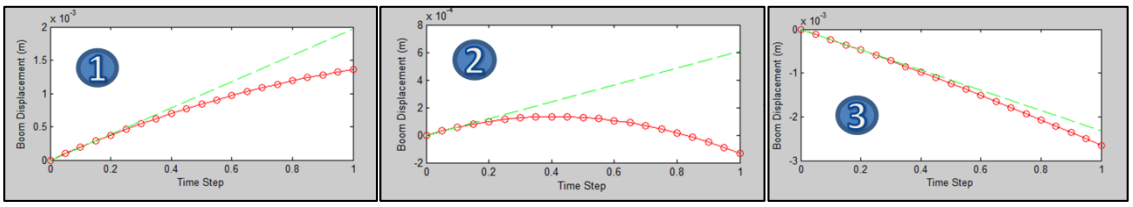

Figure 4.30 – Non-linearity Factor: three different behaviours

All three nonlinearities were captured in the design space, with some designs showing boom reversal (up and then down as well as down and then up), nonlinear boom tip deflection and aft wing buckling.

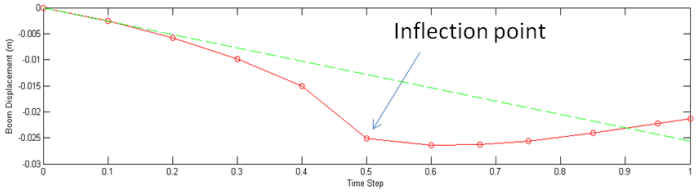

Figure 4.31 – Reverse Factor: example of inflection point

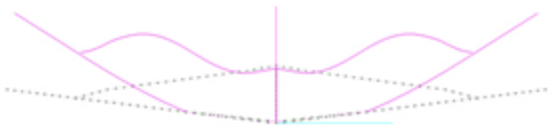

Figure 4.32 – Buckling Factor: example of the deformation plot (front view)

After an interrogation of the design space, three candidate designs were chosen, one showing the largest amount of boom reversal, one showing a large amount of boom tip softening: and one demonstrating large aft wing buckling response.

5. Conclusion & Future Work

This thesis shows that the airplane is much stiffer than what FEM calculate from the static test performed.

The matching of the High Fidelity model with a simplified beam model that improves the time of the linear runs in 60 times, not to mention how easier is to run a non-linear analysis. The maximum error of the optimization was less than 8%. With more nodes to match a lower error should be found, although the time for the optimization should also increase due to the higher number of design variables.

Linear and non-linear design spaces were explored in order to understand the possible behaviour that the Joined Wing Configuration can have. Also, these sensitivities studies revealed that for the joint variable, the FW(y) and Boom(x) have the most influence on the structure. Regarding the stiffness variables, the FW ratio wall thickness and also the FW Taper variable were observed to be the ones with the greater impact on the results. However, the combination of the FW and RW, and also FW and Boom stiffness can generate a positive or negative deflection on the boom.

The sensitivity studies showed that several nonlinearities are achievable through the variation of key structural parameters such as joint and wing stiffness. Three distinct nonlinearities were shown which include stress stiffening/softening of the boom tip deflection, a specific form of the boom nonlinearity where the boom deflects in one direction in the linear region and then reverses at higher load steps and finally aft wing buckling.

The resulting designs were then proposed as candidates to the US Air Force and Boeing™ as possible starting points for the Aeroelastically Tuned RPV design.

In order to validate the material properties used to build the HF model of the airplane, some tensile tests need to be carried out. Also, the use of a prepag carbon fibre can lead to a better resin content and also a more accurate fibre orientation on the production of the composite structures.

To know the real stiffness of the airplane, for the future it should be done an individual bending test for each part of the airplane. With the results of the FW (forward wing), RW (rear wing), boom and fuselage, it should be possible to match each part individually in a finite element program. After matching each individual part, it is possible to know the real value for the joints.

For the future of the project, there is a possibility to use a non-linear joint with a stop angle, and improve the beam model to be closer to the reality, and so, be able to capture the interaction between the boom and the fuselage skin. The Young modulus of the boom can be a variable in the optimization process in order to capture these interactions.

Also, it will be interesting to understand the effects on the aerodynamic with different types of deflections.

6. Bibliography

[1] Northrop Grumman. (2010) RQ-4 Block 20 Global Hawk. [Online]. http://www.as.northropgrumman.com/products/globalhawk/index.html [Assesed: June 7, 2015]

[2] Rasnussen, C.C., Canfield, R.A., and Blair, M., "Optimization Process for Configuration of Flexible Joined-Wing," *10th AIAA/IDDMO Multidisciplinaery Analysis and Optimization Conference*, pp. 1-9, September 2004.

[3] Lucia, D. J., "The SensorCraft Configurations: A Non-Linear AeroServoElastic Challenge For Aviation," *AIAA-2005-1943, 46th AIAA/ASME/ASCE/AHS/SCS Structures, Structural Dynamics and Materials Conference*, pp. 1-7, April 2005.

[4] Garnad-Royo, J., "Design and Evaluation of Geometric Nonlinearities using Joined-Wing SensorCraft Flight Test Article," May 6, 2013.

[5] Wolkovitch, J., "The Joined Wing: An Overview," *Journal of Aircraft*, vol. 23, no. 1, pp. 161-178, March 1986.

[6] Richards, J., "An Experimental Investigation of a Joined Wing Aircraft Configuration Using Flexible, Reduced Scale Flight Test Vehicles", PhD Thesis, University of Victoria, Victoria, BC Canada, June 2011.

[7] Kroo, I., Gallmant, J., and Smith, S., "Aerodynamic and Structural Studies of Joined-Wing Aircraft," *Journal of Aircraft*, vol. 28, no. 1, pp. 74-81, 1990.

[8] Gallman, J. W., Smith, S. C. and Kroo, I. M., "Optimization of Joined-Wing Aircraft," *Journal of Aircraft*, vol. 30, no. 6, pp. 897-905, November 1993.

[9] Gallman, J. W. and Kroo, I. M., "Strutural Optimization for Joined-Wing Synthesis," *Journal of Aircraft*, vol. 33, no. 1, pp. 214-223, January 1996.

[10] Blair, M. and Canfield, R. A., "A Joined-Wing Structural Weight Modeling Study," *14th AIAA/ASME/ASCE/AHS/ASC Structures, Tructural Dynamics, and Materials Conference*, 2002.

[11] Patil, M.J., "Nonlinear aeroelastic Analysis of Joined-Wing Aircraft," *44th AIAA/ASME/ASCE/AHS Structures, Structural Dynamics, ans Materials Conference*, pp. 1-7, 2003.

[12] Ricciardi, A., Patil, M. Canfield, R., and Lindsley, N., "Evaluation of Quasi-Static Gust Loads Certification Methods for HALE Aircraft," *Journal of Aircraft*, vol. 50, no. 2, pp. 457-468, 2013.

[13] Roberts, R. W., Canfield, R. A., and Blair, M., "Sensor-Craft Strucutral Optimization and Analytical Certificarion," *46th AIAA/ASME/ASCE/AHS/ASC Strutures, Strucutal Dynamics and Materials Conference*, 2005.

[14] Blair, M., Canfield, R. A., and Roberts, R. W., "Joined.Wing Aeroelastic Design with Geometric Nonlinearity," *Journal of Aircraft*, vol. 42, no. 4, pp. 832-848, July 2005.

[15] Bond V., "Flexible Twist for Pitch Control in a High Altitude Long Endurance Aircraft with Nnlinear Response," *Ph.D. thesis, AIR FORCE INSTITUTE OF TECHNOLOGY*, 2008.

[16] Richards, J., Aarons, T., Garnand-Royo, J. Suleman, A., Canfield, R. A. and Woolsey, C., "Airworthiness Evaluation of a Scaled Joined-Wing Aircraft," *53rd AIAA/ASME/ASCE/AHS/ASC Structures, Strutural Dynamics and Materials Conference*, pp. 1-37, 2012.

[17] Richards, J., Suleman, A., Canfield, R., and Blair, M., "Design of a Scaled RPV for Invertigation of Gust Response of Joined-Wing Sensorcraft," *50th AIAA/ASME/ASCE/AHS/ASC Stuctures, Structural Dynamics, and Materials Conference*, pp. 1-14, 2009.

[18] Keulen C., "Tensile test specimen preparation," August 31 2011.

[19] ANSYS, “ANSYS, Inc. Theory Reference, ANSYS Release 9.0”, SAS IP, Inc., USA, 2011

[20] Henri Gavin, "Structural Element Stiffness, Mass, and Damping Matrices," Duke University, 2014. [Online]. http://people.duke.edu/~hpgavin/cee541/StructuralElements.pdf, [Assesed: January 10, 2016]

[21] Afonso F., "Dynamic Scalling of a Joined-Wing Sensorcraft Configuration," MES Thesis, Instituto Superior Técnico, Universidade Técnica de Lisboa, Lisboa, Portugal, June 2011.

[22] Andrew Thomas Scott, "An evaluation of tree commercially available integrated design framework packages for use in the Space Systems Design Lab," April 2001.

[23] (2010) [Online] http://www.phoenix-int.com/software/phx-modelcenter.php. [Assesed: September 28, 2015]

[24] Mark Bigley, Candy Nelson, Peter Ryan and W. H. Manson, "Tutorials and Examples of Software Integration Techniques for Aircraft Design using ModelCenter™," 1999.

[25] (2010) [Online] http://www.mece.ualberta.ca/tutorials/ansys/. [Assesed: November 20, 2015]

[26] (2010) [Online] http://www.mathworks.com/products/matlab/. [Assesed: November 20, 2015]

[27] (2010) [Online] http://en.wikipedia.org/wiki/VBScript. [Assesed: November 20, 2015]

[28] (2010) [Online] http://office.microsoft.com/pt-pt/excel/. [Assesed: November 20, 2015]

Annex A. Measurements of coupons

Uni-directional carbon

coupon nº	1	2	3	4	5	6	7	8
thickness1	1.95	2.12	2.19	2.33	2.00	2.01	2.09	2.14
thickness2	2.06	2.10	2.13	2.21	1.94	1.97	2.10	2.16
thickness3	1.94	2.07	2.11	1.96	1.88	2.11	1.96	1.94
thickness4	2.09	2.07	1.95	2.08	2.03	2.17	1.94	1.87
thickness5	2.14	2.04	2.17	2.01	2.08	2.09	2.07	1.91
thickness6	2.09	2.18	1.92	2.31	1.95	2.12	1.95	1.99
thickness7	2.08	2.06	2.06	2.20	1.98	2.02	2.05	1.89
thickness8	2.04	2.28	2.22	2.13	2.03	2.10	2.10	1.84
thickness9	2.01	2.24	2.19	2.23	2.00	2.07	2.02	1.87
thickness10	2.06	2.17	2.09	2.14	2.08	2.14	2.11	1.95
average thickness	2.05	2.13	2.10	2.16	2.00	2.08	2.04	1.96
width1	15.47	15.46	15.54	15.47	15.6	15.31	15.35	15.64
width2	15.25	15.39	15.36	15.47	15.52	14.85	15.19	15.73
width3	15.52	15.47	15.47	15.51	15.48	13.77	15.43	15.85
average taper	0.27	0.08	0.18	0.04	0.12	1.54	0.24	0.21

Woven Carbon

coupon nº	1	2	3	4	5	6	7	8
thickness1	1.52	1.59	1.52	1.53	1.54	1.50	1.47	1.48
thickness2	1.55	1.57	1.48	1.62	1.63	1.57	1.59	1.47
thickness3	1.53	1.54	1.60	1.57	1.57	1.60	1.64	1.55
thickness4	1.61	1.53	1.51	1.67	1.61	1.64	1.58	1.50
thickness5	1.58	1.51	1.60	1.64	1.62	1.57	1.63	1.57
thickness6	1.51	1.57	1.60	1.61	1.75	1.57	1.61	1.57
thickness7	1.55	1.59	1.66	1.68	1.61	1.58	1.58	1.58
thickness8	1.61	1.61	1.67	1.60	1.60	1.52	1.63	1.60
thickness9	1.53	1.64	1.72	1.62	1.61	1.55	1.53	1.51
thickness10	1.56	1.64	1.65	1.61	1.48	1.44	1.51	1.52
average thickness	1.56	1.58	1.60	1.62	1.60	1.55	1.58	1.54
width1	15.44	15.49	15.51	15.45	15.47	15.53	15.59	15.41
width2	15.2	15.54	15.34	15.42	15.42	15.29	15.49	15.40
width3	15.53	15.5	15.47	15.48	15.48	15.48	15.47	15.49
average taper	0.33	0.05	0.17	0.06	0.06	0.24	0.12	0.09

Glass Fiber

coupon nº	1	2	3	4	5	6	7	8
thickness1	0.77	0.78	0.75	0.76	0.76	0.78	0.87	0.8
thickness2	0.8	0.78	0.75	0.8	0.83	0.84	0.85	0.75
thickness3	0.84	0.8	0.75	0.79	0.82	0.85	0.83	0.82
thickness4	0.87	0.81	0.79	0.74	0.81	0.82	0.79	0.86
thickness5	0.91	0.81	0.83	0.7	0.88	0.87	0.95	0.87
thickness6	0.93	0.83	0.81	0.74	0.89	0.81	0.78	0.78
thickness7	0.88	0.81	0.77	0.73	0.83	0.75	0.84	0.8
thickness8	0.85	0.84	0.78	0.72	0.79	0.9	0.75	0.8
thickness9	0.77	0.78	0.75	0.74	0.83	0.81	0.82	0.84
thickness10	0.78	0.74	0.78	0.75	0.84	0.82	0.82	0.77
average thickness	0.84	0.798	0.776	0.747	0.828	0.825	0.83	0.809
width1	14.82	14.84	15	14.72	14.86	14.88	14.94	14.85
width2	14.43	14.4	14.52	14.53	14.4	14.54	14.42	14.57
width3	14.83	15	14.88	14.71	14.84	14.85	15.02	14.75
average taper	0.4	0.6	0.48	0.19	0.46	0.34	0.6	0.28

Annex B. Points for building the geometry of Sensorcraft

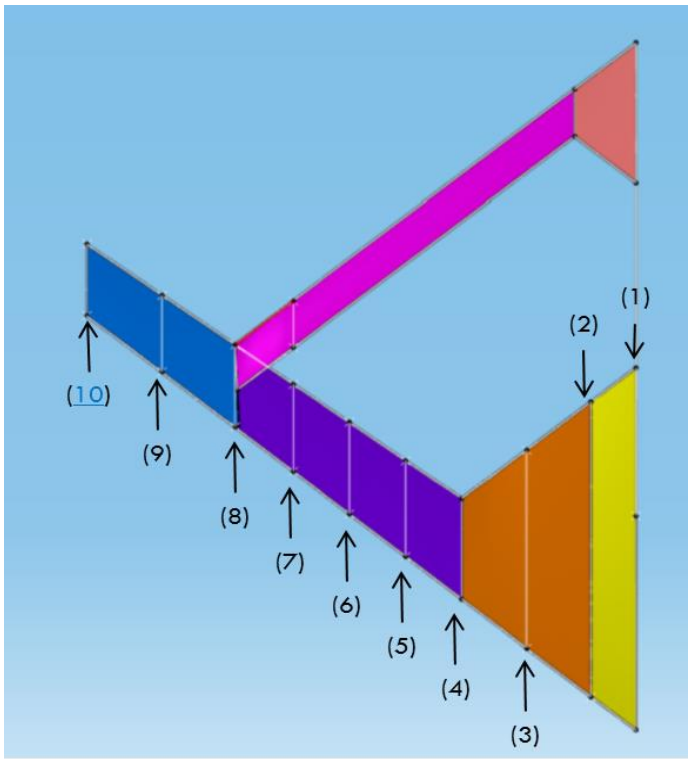

	Wing								
	Station (from Catia Meas)	1	2	3	4	5	6	7	8	9
Inboard	x location of inboard section	0	0.16	0.39	0.62	0.82	1.02	1.22	1.43	1.69
	y location of inboard section	0	0.21	0.5	0.79	1.05	1.3	1.56	1.83	2.16
	z location of inboard section	0	0.03	0.07	0.1	0.13	0.16	0.19	0.22	0.25
	Chord Length	1.71	1.39	0.93	0.48	0.45	0.43	0.41	0.39	0.36
	Twist	-0.01	0.04	0.06	0.08	0.07	0.05	0.02	0.03	-0.03
	Station (from Catia Meas)	2	3	4	5	6	7	8	9	10
Outboard	x location of outboard section	0.16	0.39	0.62	0.82	1.02	1.22	1.43	1.69	1.95
	y location of outboard section	0.21	0.5	0.79	1.05	1.3	1.56	1.83	2.16	2.5
	z location of outboard section	0.03	0.07	0.1	0.13	0.16	0.19	0.22	0.25	0.29
	Chord Length	1.39	0.93	0.48	0.45	0.43	0.41	0.39	0.36	0.34
	Twist	0.04	0.06	0.08	0.07	0.05	0.02	0.03	-0.03	-0.09

Strut		
	Station (from Catia Meas)	11
Inboard	x location of inboard section	1.01
	y location of inboard section	0
	z location of inboard section	0.01
	Chord Length	0.7
	Twist	0.000
1	Station (from Catia Meas)	12
Outboard	x location of outboard section	2.57
	y location of outboard section	0
	z location of outboard section	0.52
	Chord Length	0.66
	Twist	0.000

Aft Wing				
	Station (from Catia Meas)	12	13	14
Inboard	x location of inboard section	2.57	2.79	1.8
	y location of inboard section	0	0.28	1.56
	z location of inboard section	0.52	0.47	0.29
	Chord Length	0.66	0.22	0.22
	Twist	0.00	0.00	0.05
	Station (from Catia Meas)	13	14	15
Outboard	x location of outboard section	2.79	1.8	1.6
	y location of outboard section	0.28	1.56	1.82
	z location of outboard section	0.47	0.29	0.21
	Chord Length	0.22	0.22	0.21
	Twist	0.00	0.05	-0.017453